Computers and Geotechnics 118 (2020) 103363

Contents lists available at ScienceDirect

Computers and Geotechnics

journal homepage: www.elsevier.com/locate/compgeo

Research Paper

A study on Bonded Block Model (BBM) complexity for simulation of laboratory-scale stress-strain behavior in granitic rocks

Sankhaneel Sinha*, Gabriel Walton

Department of Geology and Geological Engineering, Colorado School of Mines, 1516 Illinois St., Golden, CO, United States

ARTICLE INFO

Keywords:
Bonded block models
Voronoi tessellation
Rock fracturing
Model complexity

ABSTRACT

The emergent macroscopic behaviors of Bonded Block Models (BBM) are governed largely by the properties assigned to their three components – blocks, contacts and zones (blocks are discretized using finite-difference zones). Over the years, different representations of these components, including elastic/inelastic zones and heterogeneous/homogenous blocks and contacts (corresponding to different mineral grains and associated mechanical properties), have been employed to simulate various aspects of rock behavior. However, there is a lack of understanding of the capabilities of these model representations with respect to their ability to replicate specific rock mechanical attributes. The goal of this study was to test a variety of model representations and evaluate their capabilities in terms of reproducing mechanical behaviors observed for a granitic rock type.

It was found that inelastic zones were necessary to capture high confinement peak strengths while incorporation of heterogeneity was necessary to replicate the micro-cracking process. The heterogeneous, inelastic BBMs could match all the calibration targets and is identified as the best representation for modeling the full range of granitic rock behaviors. To help researchers select an appropriate BBM representation for modeling different aspects of rock behavior, a summary table outlining the capabilities of the different model representations is also provided.

1. Introduction

Grain-scale microstructures in crystalline rocks are known to control their emergent macroscopic mechanical response to loading [102,54,35]. When such rocks are loaded under compression in a laboratory setting, a heterogeneous stress field is created within the specimen due to the elastic mismatch among constituent grains and the presence of micro-flaws (pores, cleavages, strings of grain boundary cavities; [88,90,23,53,54]). As the local tensile strength in the vicinity of a flaw or at a grain boundary is eventually exceeded, new microcracks are created [41,23,53,13,25]. The microcracks continue to grow and coalesce with loading, ultimately leading to macroscopic failure via axial splitting (under unconfined conditions) or shear band development (under high confinement; [11,64,30]). The overall damage evolution therefore hinges on the complex interaction between microcracks and the stress field.

The microstructure of a rock is generally characterized by grain size, grain shape, grain types and their distributions, contact properties, elastic properties and crystallographic orientations [37]. Lan et al. [54] describes three sources of microstructural heterogeneity: (a) Geometric: due to variability in shape and size of the grains, (b) Elastic: due to stiffness contrast of constituent minerals, and, (c) Contact: due to variable length, orientation and mechanical properties of grain contacts. Although the influence of geometric heterogeneity has been studied using experimental techniques in the past [74,50,101,31], the number of polygonal block-based and grain-based modeling studies that investigate additional aspects of heterogeneity has increased rapidly in recent years [54,17,75,1,59,105].

The grain-scale modeling approach is a sub-set of the Discrete Element Method (DEM; [21]), and essentially represents a material space using aggregates of detachable blocks. Two important attributes that have led to its widespread acceptance are the general resemblance in shape of the modeled blocks to actual mineral grains and the ability of the modeling methods to allow for realistic fracture formation and opening. Over the years, this modeling approach has been successfully used in reproducing various features of the rock damage process [52,54,45,10,7,33,35,17,67,75,105,57]. The polygonal block shape has also been recently incorporated in the Finite Discrete Element Method (FDEM) framework to improve the grain representations [1]. Details on FDEM and its application in small and large-scale rock engineering problems can be found in Munjiza [70], Mahabadi [61], Mahabadi et al. [62], Mahabadi et al. [63], Lisjak et al. [58], etc.

* Corresponding author.
E-mail address: sankhaneelsinha@mymail.mines.edu (S. Sinha).

https://doi.org/10.1016/j.compgeo.2019.103363
Received 11 August 2019; Received in revised form 19 November 2019; Accepted 20 November 2019
Available online 27 November 2019
0266-352X/

In DEM models, different approaches exist for representing the grains/blocks and their respective contacts. Particle Flow Code Grain-based models (PFC-GBMs) use a combination of bonded circular/spherical particles [81] in the grains and smooth-joints [65] along the grain contacts. Alternatively, polygonal or triangular GBMs, popularly known as Bonded-Block Models (BBMs), employ a continuum mesh within the blocks and a Coulomb-slip model for the block contacts [51]. As pointed out by Gao et al. [39], PFC-GBMs have a high intrinsic porosity due to the spherical shape of the particles and it is difficult to model low porosity rocks with this approach. BBMs, on the other hand, have a highly interlocked block structure and as such do not suffer from the porosity issue. While both these approaches are capable of realistically replicating the rock fracturing process (e.g. [54,35,98,105] etc.), this study will focus only on the BBM approach.

A BBM developed to mimic a multi-minerallic rock should ideally incorporate all sources of micro-structural heterogeneity discussed above. Yet previous BBM studies have adopted some major simplifications that neglect one or more sources of heterogeneity. For example, Ghazvinian et al. [45] employed a homogenous block model (uniform block and contact properties) to reproduce the Unconfined Compressive Strength (UCS), Young's modulus (E) and Poisson's ratio (ν) of Lac du Bonnet granite. The same rock was simulated using a mineralogically heterogeneous BBM (4 mineral block types and 10 contact types) by Farahmand and Diederichs [35], and that model was able to reproduce UCS, E, ν, triaxial strengths, and pre-peak cracking thresholds (Crack Initiation and Crack Damage thresholds). It is apparent that the BBM in Farahmand and Diederichs [35] was more complex and accordingly could reproduce more macroscopic rock attributes/properties (as recorded in the laboratory) than those in Ghazvinian et al. [45]. Since each of the previous BBM studies have employed a single model setup and demonstrated match to certain rock attributes, the relationship between model complexity and its ability or inability to capture other aspects of rock mechanical behavior is not well understood.

In this study, we attempt to identify the degrees of model complexity that are necessary to replicate a variety of rock behaviors. To this end, a large suite of laboratory-derived mechanical properties for a granitic rock were identified, and attempts were made to replicate as many of these properties (referred to as calibration targets herein) as possible using different model representations. The model results presented were calculated using input parameters that were obtained through an iterative manual back-analysis process.

2. Review of pertinent literature

The grain-based modeling approaches only started to receive attention in the last decade, as means to overcome the drawbacks of the Bonded Particle Method (BPM). BPM was developed by Cundall and Strack [22], Potyondy et al. [79], Diederichs [24] and Potyondy and Cundall [81] and is the precursor to most of the micromechanical modeling techniques available today. In BPM, a material is represented by an assemblage of circular discs or spheres that interact via parallel bonds and linear contact laws. Since its introduction, a number of limitations were identified in BPM [18] and modifications were proposed to overcome these limitations [81,18,80,83,28]. Most of these modifications identified the lack of particle-particle interlocking in BPM and tried to overcome them by fusing neighboring spheres/discs.

The polygonal grain-based modeling approach, typically applied using Voronoi Tessellations, attempts to better represent the geometric characteristics of polycrystalline rocks, and as such does not suffer from the lack of particle interlocking [45,67]. As described in Section 1, there are two popular ways of defining the polygonal grains: PFC-GBM and BBM. PFC-GBM, as the name suggests, is typically built using the Itasca software PFC2D or PFC3D. BBM, on the other hand, operates using the UDEC or 3DEC software.

The block zones in BBM can be assigned either an elastic or an inelastic constitutive model; if inelastic, then appropriate strength parameters like cohesion, friction angle, tensile strength have to be defined. The 'contacts' between neighboring blocks operate per the Coulomb slip model and are characterized by deformational (stiffness) and strength (cohesion, friction angle and tensile strength) parameters. Since its emergence, the 2-dimensional UDEC-BBM has been widely used to study micro-fracturing in rocks [19,54,38,33,35,72,15,91,39,75,56,6,85,57], scale effects in rocks [73,89], damage around tunnels and underground excavations [20,38,84,8], spalling in rock pillars [82,85], etc. Similar studies have been conducted using its 3-dimensional counterpart, i.e. 3DEC-BBM (e.g., [45,42,43,98,99]).

In BBM, the individual blocks typically are either polygons with four or more sides (Voronoi) or triangles (Trigon). The Voronoi blocks are more representative of the petrographic characteristics of crystalline rocks, but there has been some success in modeling granites using Trigons as well [38,39]. A key issue with the use of Trigons is the resulting predisposition towards shear fracturing due to the availability of linear failure pathways [45,67,85]. As we move towards broader application of BBM, there are concerns that Trigon BBM may not have the capability to properly represent volumetric deformation even when strength is accurately captured [86]. It follows that Voronoi BBM, because of its interlocking capabilities, might be better suited for studying the deformation and damage in brittle geomaterials.

Although Voronoi BBM has shown promise in various domains of rock engineering, the focus of this study is on laboratory-scale modeling efforts. As indicated above, there have been a large number of attempts to model the progressive fracturing process in rocks under compression. When considering such prior works (see summary Table 1), it is interesting to note the various representations of zones, blocks and contacts that have been employed historically to model the same rock type. For example, Lac du Bonnet granite was modeled using homogenous, elastic BBMs by Ghazvinian et al. [45], homogenous, inelastic BBMs by Noorani and Cai [72] and heterogeneous (blocks and contacts) elastic BBMs by Lan et al. [54], Nicksiar and Martin [71], Chen and Konietzky [15], Farahmand and Diederichs [35] and Park et al. [75]. Within this latter category (homogenous, elastic BBM), two different contact representations were used: Lan et al. [54], Nicksiar and Martin [71] and Park et al. [75] assigned different stiffness values to contacts based on the pairs of bounding mineral blocks, but assigned the same strength parameters to all the contacts. Farahmand and Diederichs [35] and Chen and Konietzky [15], on the other hand, assigned different stiffnesses as well as strength properties to each group of contacts. Clearly, the BBMs in Farahmand and Diederichs [35] and Chen and Konietzky [15] are more complex than those in Lan et al. [54], Nicksiar and Martin [71] and Park et al. [75], in the sense that there are more input parameters in their models. It is also evident from Table 1 that as the models became more complex, a larger number of calibration targets could be matched. To better understand the relationship between BBM representation and its capabilities, this study selects granitic rock as a starting point, since granite is the most widely modeled rock type using BBM.

Laboratory-scale BBMs are, like all models, an approximation of reality – the question is what level of approximation (or conversely, model complexity) is acceptable for a particular problem in hand? To answer this question and lay the groundwork for BBMs developed as a part of this study, results from previous BBM studies have been examined. Before delving deeper into the BBM literature, a quick overview of the progressive rock-damage process is presented [64]:

(1) Under compression, rocks initially behave in a non-linear fashion due to closure of pre-existing cracks.
(2) This is followed by a linear response where the rock behaves as a fully elastic material.
(3) At around 30–50% of the peak strength, micro-cracks orientated sub-parallel or parallel to the direction of major principal stress starts forming randomly within the volume of the specimen. This stress level is termed as the Crack Initiation (CI) threshold.

Table 1
Summary of previous BBM studies. Boxes are left blank where relevant information was not provided.

Rock Type	Blocks & Contacts	Zones	2D/3D	E, ν	UCS	Triaxial Strengths	Tensile strength	Crack Initiation	Crack Damage	Stress-strain (unconfined)	Stress-strain (confined)	Reference
Granite	Homogenous	Rigid	2D	✓	✓	$\sigma_3 \leq$ 10% UCS	✓			Brittle	Hardening	Kazerani and Zhou [52]
Granite	Homogenous	Rigid	3D	✓	✓	$\sigma_3 \leq$ 10% UCS	✓	✓ [a]	✓ [a]	Brittle	Hardening	Wang and Cai [99]
Sandstone	Homogenous	Elastic	2D	✓	✓	$\sigma_3 \leq$ 35% UCS	✓			Brittle	Hardening	Bahaaddini and Rahimi [6]
Marble	Homogenous	Elastic	2D	✓	✓							Norouzi et al. [73]
Granite	Homogenous	Elastic	3D	✓	✓			✓ [a]		Brittle		Ghazvinian et al. [45]
Strong Rock [d]	Homogenous	Elastic	2D	✓	✓	$\sigma_3 \leq$ 10% UCS	✓			Brittle	Hardening	Stavrou and Murphy [89]
Granite	Homogenous	Elastic	3D	✓	✓	$\sigma_3 \leq$ 10% UCS	✓	✓ [a]	✓ [a]	Brittle	Hardening	Wang and Cai [99]
Granite	Homogenous	Inelastic	2D	✓	✓	$\sigma_3 \leq$ 30% UCS	✓		✓ [a]	Brittle		Noorani and Cai [72]
Granite	Homogenous	Inelastic	3D	✓	✓	$\sigma_3 \leq$ 10% UCS	✓	✓ [a]	✓ [a]	Brittle	Brittle (realistic)	Wang and Cai [99]
Sandstone	Heterogeneous	Elastic	2D	✓	✓		✓			Brittle		Li et al. [56]
Granite	Heterogeneous [e]	Elastic	2D	✓	✓			✓ [a]	✓ [a]			Lan et al. [54]
Granite	Heterogeneous [e]	Elastic	2D	✓	✓			✓ [a]	✓ [a]			Nicksiar and Martin [71]
Granite	Heterogeneous	Elastic	2D	✓	✓	$\sigma_3 \leq$ 10% UCS	✓	✓ [b]	✓ [b]	Brittle	Hardening	Farahmand and Diederichs (2015)
Granite	Heterogeneous	Elastic	2D	✓	✓		✓					Chen and Konietzky [15]
Granite	Heterogeneous	Elastic	2D	✓		σ_3 = 30 MPa					Hardening	Chen et al. [17]
Granite	Heterogeneous [e]	Elastic	2D	✓	✓		✓	✓ [a]	✓ [a]	Brittle		Park et al. [75]
Granite	Heterogeneous	Elastic	2D	✓	✓	$\sigma_3 \leq$ 16% UCS	✓	✓ [c]	✓ [c]	Brittle	Hardening	Li et al. [57]

✓ – matched.
[a] For unconfined conditions.
[b] For $\sigma_3 \leq$ 10% UCS.
[c] Underestimated.
[d] Properties similar to granite.
[e] Contacts have homogenous strength & heterogeneous stiffness.

(4) As loading continues, micro-cracks start to interact and coalesce at around 70–90% of the peak strength. This is called the Crack Damage (CD) threshold and marks the yield point of the rock.
(5) Microcracks continue to coalesce and grow until a macroscopic shear plane is formed across the specimen. This is followed by a rapid drop in axial load. A homogenous BBM with rigid blocks is the simplest model representation with the least number of input parameters. Such models neglect grain deformation and have been used under the pretext that mineral blocks are stiffer than the block contacts and so their deformability can be neglected [52]. Wang and Cai [99], in a recent study, showed that BBM with rigid blocks perform in a similar manner to elastic block models. With that in mind and noting the phenomenological similarity between rigid blocks and elastic blocks with high modulus, the rigid block representation was not considered explicitly in this study.

The homogenous, elastic BBM has been successfully used to replicate the elastic constants (E and ν), UCS, triaxial strengths and tensile strengths (σ_t) of various granites (UDEC-BBM: [89]; 3D-BBM: [45,99]), sandstones [6] and marbles [73]. Interestingly, the only studies that report matching CI and CD are Ghazvinian et al. [45] and Wang and Cai [99], and both these studies were conducted in 3D.

From a mechanistic perspective, elastic blocks imply unbreakable mineral grains, meaning that these models should be capable of simulating conditions where damage occurs predominantly via grain boundary fracturing (i.e. inter-granular) rather than via intact grain damage (i.e. intra-granular or trans-granular). Previous fundamental studies on rocks have found micro-fracturing to initiate at grain-boundaries under unconfined and low confinement conditions, with the density of intra-granular fractures increasing with confining stress [88,90,100,53,32,46,60]. The change in mode of fracture formation with confinement is also generally consistent with recent GBM studies [49,76,1]. Note that for the purposes of this study, the terms 'intra-granular' (existing within a grain; [53] and 'transgranular' (crossing multiple grains; [53]are not differentiated because of the difficulty of identifying them in BBM; instead, the umbrella term 'intra-granular cracks' is used throughout.

It follows that elastic homogenous BBMs should be capable of representing the peak strengths under unconfined and low-confinement conditions only. This is confirmed by the fact that former BBM studies considering granites have either not reported triaxial simulation results (e.g. [45]) or performed calibration for a limited range of confinement (e.g. 0–10% UCS). Additionally, the strength envelopes were almost perfectly linear, implying that models ran at higher confinements would likely lead to peak strengths larger than expected in reality.

Noorani and Cai [72] modified the zone constitutive model to strain-softening type, with the goal of capturing the combined effect of grain boundary and intra-granular fracturing in BBM. The use of a softening constitutive model allows the zones to deform inelastically upon yield, which is phenomenologically equivalent to grain damage. This approach was shown to be capable of capturing the UCS, tensile strength, triaxial strengths up to σ_3 = 30% UCS, CD under unconfined conditions, and the general phenomenon of reduced dilatancy at higher confinement. However, due to the homogenous nature of the specimen, it is likely that the unconfined and confined CIs (these values were not reported in the study) and the confined CDs were not replicated in these models.

With respect to the representation of the intra-granular fracturing process, a sub-tessellation approach was demonstrated by Gao et al. [39] and Wang and Cai [98]. In that approach, each mineral block was further split into sub-blocks, and grain damage was represented by cracking along the sub-block contacts. Such an approach is appealing, since it allows for explicit simulation of intragranular fracturing. This approach does have two major limitations, however: (1) Creation of sub-blocks increases the computational demands and model runtime drastically; (2) A small number of sub-blocks (5–6) enforces kinematic constraints on where fractures can develop within a particular block. Accordingly, where it is not computationally feasible to generate a large number of sub-blocks (see [1]), a potential alternative is to utilize continuum zones with an inelastic constitutive model to approximate intragranular damage.

The introduction of different mineral blocks and contacts are means of incorporating stiffness heterogeneity within BBMs. Dey and Wang [23] have shown that the stiffer mineral at a welded contact experiences additional boundary traction when an external stress is applied to the system. If these stresses exceed the local tensile strength at the contact, new grain boundary cracks form. In BBM, since it is not possible to include microscopic flaws (cavities, pores) at grain-boundaries, initiation of microcracking is governed mainly by grain movements (translation and rotation; [45]) and elastic property mismatch. While the contribution of elastic property mismatch towards generation of local tensile stress is negligible in homogenous BBMs, the effect is pronounced in heterogeneous BBMs. Accordingly, most of the heterogeneous BBM studies in the literature have been able to match the unconfined CI threshold [54,71,75]. [35] went a step further by demonstrating that heterogeneous, elastic BBMs can capture CI under confined conditions as well.

With respect to peak strength in heterogeneous models, Lan et al. [54], Nicksiar and Martin [71], Chen and Konietzky [15] and Park et al. [75] only report calibration under unconfined conditions, whereas, Farahmand and Diederichs [35] and Chen et al. [17] show triaxial results up to σ_3 = 10% UCS. The strength envelopes were linear because of the elastic nature of the blocks. From the literature survey, it was not possible to identify the relative benefits of assigning different strength properties to only the block contacts, as the studies employing the homogenous contact strength simplification (e.g., Lan et al. [54,75]) did not report triaxial simulation results.

A peculiar behavioral aspect of elastic BBMs is the notable pre-peak hardening after yield under confined loading [35,17,6,57,99]. In a real rock, grain boundary fractures connect via intra-granular fractures, resulting in shorter pre-peak hardening phases. In absence of such grain fracturing capabilities, a longer fracture path along the blocks contacts has to be followed in elastic BBMs that ultimately result in an extended hardening phase. This drawback can be overcome if the zones within the blocks are allowed to yield and soften [99,87,86].

A review of literature has provided some insight into the strengths and limitations of the different model representations in BBM and has also helped identify research questions that remain unanswered to date. A key problem with drawing conclusions on the basis of the previous studies is the lack of similitude in their methodologies (e.g. loading mechanism, boundary conditions, 2D vs 3D, different rocks and calibration targets), and the absence of any discussions pertaining to the inabilities of the respective BBMs. To allow for a more quantitative comparison and to accomplish the ultimate goal of determining the optimum level of model complexity for various applications, a granite and its associated geomechanical parameters were selected, and attempts were made to reproduce as many attributes as possible with the various BBM representations.

3. Laboratory data

The rock selected for this study is from the 7910 ft (2.4 km) level of Creighton mine located in Sudbury, Canada. The mineralogical composition of the footwall rocks collectively referred to as "Creighton Granite" varies, but they are all treated as a single geomechanical unit [93]. The average petrographic composition is approximately 30% Quartz, 55% Na-Feldspar and 15% Biotite [87,86]. The mineral grains are highly irregular in shape with an average size of 2.25 mm [87,86].

Uniaxial and triaxial (0–60 MPa confinement) compression tests as well as Brazilian tensile tests were conducted on Creighton Granite samples in the CANMET Natural Resource Laboratory in Ottawa, Canada and the results were previously analyzed by Walton [93]. The

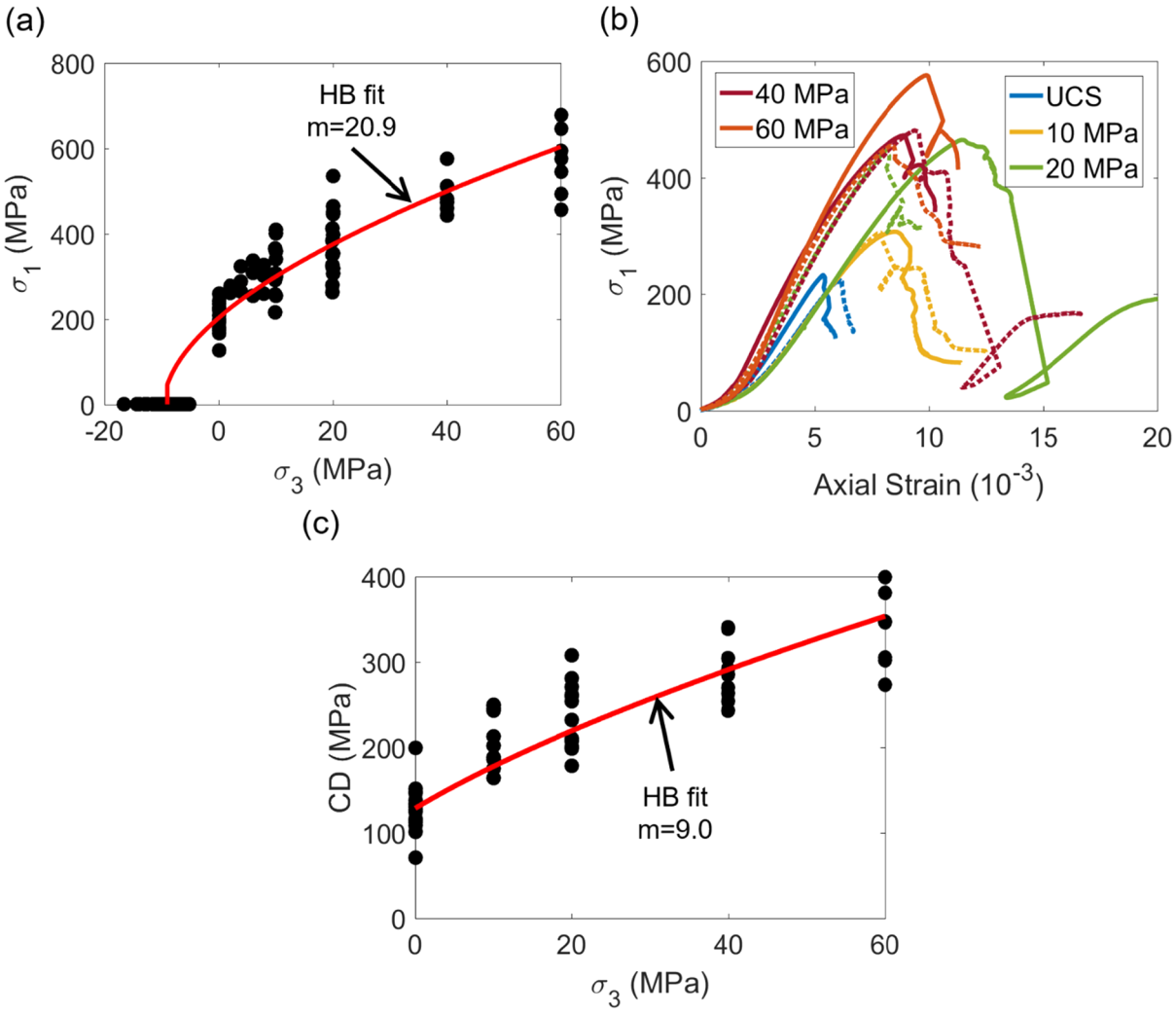

Fig. 1. (a) Peak strengths [93], (b) Two laboratory stress-strain curves for each level of confinement (one solid and one dashed) and, (c) Crack Damage thresholds.

average UCS is 203 MPa and the average direct tensile strength (estimated by applying a correction factor to indirect Brazilian tensile strength data per the findings of Perras and Diederichs [78] is 9 MPa. The high UCS/σ_t ratio (23) is an indication of the brittle nature of the rock, and reflects the high spalling potential for the rock [26]. The Hoek-Brown (HB) failure envelope was fitted to the dataset following the guidelines of Hoek and Brown [48] to obtain an m_i of 20.9 [93]. The peak strengths and some representative laboratory stress-strain curves are shown in Fig. 1a and b. For each test, the axial and the lateral strains were recorded in real time to allow for the characterization of CI, CD and volume changes in the specimens; although Walton [93] did not previously report CI and CD values for Creighton Granite, they were estimated for this study as described below.

CD is commonly accepted as the long-term strength of the rock and is defined as the point of non-linearity in the axial stress-axial strain curve [64,26,27]. CD can also be identified as the point of volumetric strain curve reversal (only for unconfined conditions; [25]) or by monitoring acoustic emissions from the rock specimen [29]. Since no acoustic data was available for Creighton granite, CD was determined from the axial stress-strain curve based on the point of onset of tangent modulus decrease [25,95,97] and is shown in Fig. 1c. The mean unconfined CD is 128.7 MPa, which is only 63% of the mean UCS. This value is closer to the lower limit of CD thresholds typically observed in granitic rocks [11,107,103,77].

The CI threshold marks the onset of extensile microcracking in the rock specimen and is identified as the point of crack-volumetric strain reversal [64,97,77] or non-linearity in the axial strain-lateral strain curve [44]. The calculation of crack volumetric strain is dependent on the elastic constants (i.e. Young's Modulus and Poisson's ratio), and is particularly sensitive to changes in Poisson's ratio [29]. Most of the axial stress – lateral strain curves for Creighton granite exhibited marked non-linearity from the beginning of each test (likely due to crack-closure). The behavior was more pronounced in the confined test curves, which made it difficult to reliably estimate a Poisson's ratio.

As an alternative, the Inverse Tangent Lateral Stiffness (ITLS) method [44] was used to determine the CI thresholds. The advantage of this approach is that it relies solely on the shape of the axial stress-lateral strain curve for identifying the CI. The inverse tangent lateral stiffness can be calculated using the following equation [44]:

$$\varepsilon_l \Delta = \frac{\Delta \varepsilon_l}{\Delta \sigma_1} \tag{1}$$

where $\Delta\sigma_1 = \sigma_{i+8} - \sigma_{i-8} (i = 1, 2, 3\cdots)$ and σ_i is the i^{th} axial stress datapoint, $\Delta\varepsilon_l = \varepsilon_{li+8} - \varepsilon_{li-8} (i = 1, 2, 3\cdots)$ and ε_{li} is the i^{th} lateral strain datapoint.

The recommended bin size of 16 can be modified depending on the resolution of test data. In this study, the bin size of 16 was employed following a moving average analysis to reduce the noise in the ITLS values. Fig. 2a shows one such graph from a UCS test plotted against σ_1. The point where the ITLS starts to deviate from linearity (marked by a green circle in Fig. 2a) is CI. The CI thresholds determined using the ITLS approach are shown in Fig. 2b, along with the best-fit line.

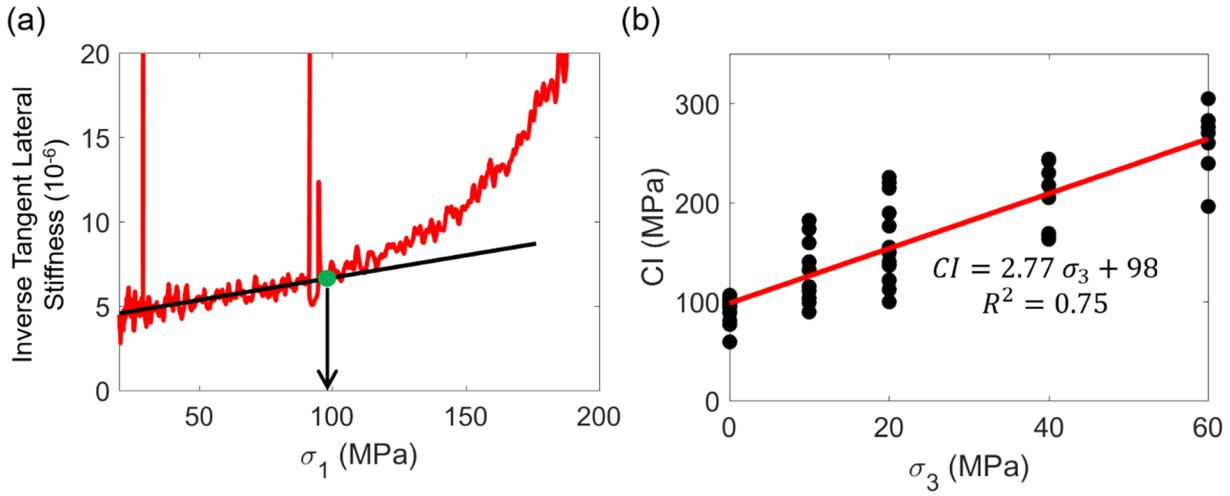

Fig. 2. (a) Inverse Tangent Lateral Stiffness (ITLS) method for identifying CI demonstrated for unconfined test data, (b) Crack Initiation threshold determined using the ITLS method.

Interestingly, the coefficient of the confinement term in the CI equation is 2.77, which is nearly double what Diederichs [25] obtained ($\sigma_1 = 90 + 1.4\sigma_3$) through back-analysis of in-situ damage observations at the Creighton mine. Walton and Diederichs [96] also found a constant deviatoric CI threshold to reasonably replicate the damage evolution in a pillar at Creighton mine. On the contrary, this study as well as those by Chang and Lee [14] and Peng et al. [77] have obtained a much higher confinement dependency from laboratory tests on granites. The exact cause for this disconnect between laboratory data and in-situ observations is not well understood and is a topic for future research. One possible reason could be the generation of Hoop stresses in the specimen that delays the onset of stable cracking [26]. This rationale, however, does not conform with the assertion that CI is a material-specific stress threshold and as such should be unaffected by boundary conditions and testing geometries [26,27].

With respect to elastic properties, Walton [93] noted a modest confinement dependency of the Young's modulus, with average values ranging from 52.7 GPa (for UCS) to 79.7 GPa (for $\sigma_3 = 60$ MPa). This variability was explained as an effect of pre-damage caused by stress relaxation as the core samples were being extracted. The upper limit of the modulus is therefore most likely to be indicative of the intact in-situ rock behavior. However, since the specimens tested in laboratory were already pre-damaged, and recalling that BBMs are zero porosity systems with no simple method to incorporate open cracks, for the purposes of comparison with BBM models, we will use the mean Young's modulus across the range of confining stresses considered. Arzúa et al. [5] and Walton et al. [95] suggested that in brittle rocks, the confinement dependency of elastic modulus can be mathematically represented by a logarithmic function that transitions to a linear function below a certain confinement (see Eq. (2)).

$$E(\sigma_3) = E_o + \begin{cases} \frac{\omega' \sigma_3}{e^{(\frac{\omega' + \omega_0}{\omega'})}} \; when \;\; \sigma_3 < e^{(\frac{\omega' + \omega_0}{\omega'})} \\ \omega' \ln(\sigma_3) - \omega_o \; when \;\; \sigma_3 > e^{(\frac{\omega' + \omega_0}{\omega'})} \end{cases} \quad (2)$$

where E_o is the mean elastic modulus under unconfined condition, ω' and ω_o are fit parameters. Walton [93] reported the fit parameters for Creighton granite to be 13.91 and 29.31, respectively. In order to obtain a representative modulus value, Eq. (2) was integrated from $\sigma_3 = 0 - 60$ MPa and then divided by 60 MPa, which gave a value of 69 GPa. This value was considered as the calibration target for the BBMs.

The average Poisson's ratio for Creighton granite was calculated to be 0.26 (with a standard deviation of ~0.03). Walton and Diederichs [96] had previously reported a Poisson's ratio of 0.1 for Creighton granite. The discrepancy in the values is attributed to the methodologies opted in the two studies – Walton and Diederichs [96] selected the stress range for calculating the Poisson's ratio from the initial linear section of the axial stress – lateral strain curve while here we chose the stress range from the linear section of the axial stress – axial strain curve per ISRM guidelines [12,34]. It is not clear which of the two techniques provides a better estimate of Poisson's ratio, given that the initial linear section of axial stress – lateral strain curve includes some degree of crack closure in axial strain while the linear section of the axial stress – axial strain curve often exceeds the CI threshold of the rock. In other words, the stress range in which the rock behaves in an elastic manner sometimes do not concur in the axial strain and lateral strain space.

4. Model setup and description

The applicability of BBMs for simulation of brittle damage in Creighton granite was tested through a series of simulated Brazilian, UCS and triaxial tests in the explicit distinct element software UDEC. Fig. 3 shows the geometry of the Brazilian and UCS / triaxial model setup. The Brazilian sample is 55 mm in diameter and was loaded through two steel platens on either side. The UCS / triaxial sample is 120 mm in height and 55 mm in width, and was loaded via a constant velocity boundary along the model top. In both sets of models, the bottom was restrained by roller boundaries. The laboratory stress-strain curves had controlled post-peak behavior that implies that the loading system was very stiff; as a result, no platens were included in the UCS / triaxial models, which effectively simulates an infinitely stiff loading system. The lack of any lateral constraints or platen friction on the specimen ends simulates a frictionless platen condition; with that said, previous studies have found the effect of platen friction on test results for slender specimen geometries (length/width ≥ 2) to be negligible [68,47,40].

In the triaxial simulations, the hydrostatic stress was first applied to the specimen, followed by the application of deviatoric loading. The loading velocity was 0.005 m/sec for the Brazilian test and 0.01 m/sec for the UCS / triaxial models. Although these values are large in comparison to the typical loading rates in laboratory tests, the time step itself is extremely small in UDEC [51]. This means that a large number of solution steps are required for displacing the boundaries by unit distance. The velocities chosen are small enough to mimic a pseudo-static loading condition and are consistent with those used by Kazerani and Zhao [52], Fabjan et al. [33] and Starvou and Murphy [89]. Also,

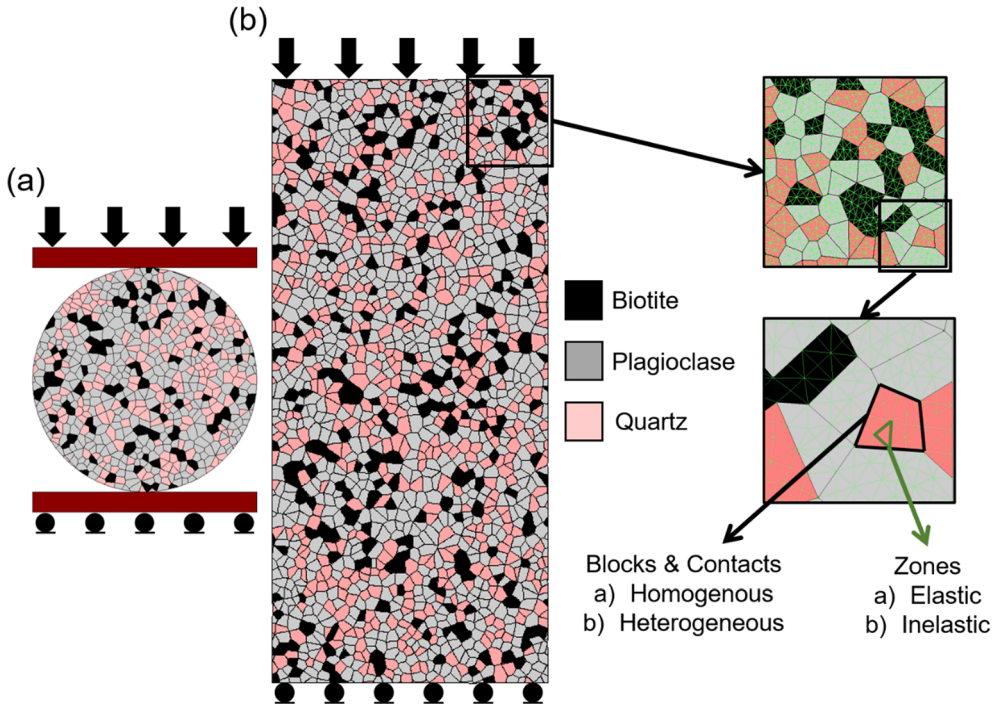

Fig. 3. Brazilian and Uniaxial / triaxial model setup (after [87,86]).

the default 'Local' damping mode in UDEC was employed in all the models in this study [51].

Many previous studies (e.g., [91,56,75]) have incorporated true grain morphologies derived from SEM or digital image processing techniques [57] in grain-based models. As pointed out by Wang and Cai [98], BBMs with block structures that are statistically similar to the actual grain size distribution of the target rock unit are often computationally intensive and impractical for calibration. At a minimum, however, the average block size should be close to the mean grain size of the rock. Given that this study encompasses a large number of model calibrations and that the geomechanical attributes correspond to rocks with slightly different petrographic characteristics, no attempt was made to incorporate the 'true' grain size distribution in the BBMs. Instead, a block edge length of 2 mm was selected that gave an equivalent average block diameter of 2.25 mm [87,86]. The blocks were then segregated into three mineral classes using a randomization scheme. This resulted in areal mineral proportions of 15.0%, 29.9% and 55.1% for Biotite, Quartz and Plagioclase, respectively. Note that the built-in Voronoi generator in UDEC tends to create a near-uniform grain size distribution [55]. Even with a very low value of 'iteration', elongated blocks for Biotite minerals could not be created; therefore, the blocks in the model do not truly represent mineral grains.

In UDEC, a block can be defined as rigid or deformable; if deformable, the blocks are discretized using constant strain triangular zones [51]. The zones can be set to behave elastically or inelastically, depending on the constitutive model assigned to them. For this study, the ratio of block to zone edge length was chosen to be 2, based on the recommendation of Fabjan et al. [33]. In addition to the zone strength properties, a complete BBM description includes zone elastic properties and contact properties. The input properties could either be uniform across the entire model (termed as homogenous) or different for different mineral blocks and their respective contacts (termed as heterogeneous). Incorporation of block/contact heterogeneity and/or zone inelasticity increases the number of input parameters and thereby amplifies the non-uniqueness issue in BBMs. From a mechanistic standpoint, however, the added complexities may be necessary to capture some well documented aspects of the rock failure behavior. When model complexity is increased, it is of course necessary to increase the number of macroscopic calibration targets as the number of input parameters increases.

To comprehend the relative benefits of increasing model complexity, the following combinations were tested: (a) Elastic zone with homogenous blocks and contacts, (b) Inelastic zones with homogenous blocks and contacts, (c) Elastic zones with heterogeneous blocks and contacts, and, (d) Inelastic zones with heterogeneous blocks and contacts. Results from one supplementary case are also presented in addition to those listed above: elastic zones with heterogeneous blocks but homogenous contacts. The rationale behind opting for a slightly simpler representation with respect to those in Lan et al. [54], Nicksiar and Martin [71] and Park et al. [75] was to isolate the effect of block heterogeneity.

For each level of model complexity, the BBM input parameters were adjusted to match as many laboratory-derived attributes as possible. The calibration methodology is similar to those in Ghazvinian et al. [45], Farahmand and Diederichs [35] and Wang and Cai [99], and is briefly described below:

(a) For the homogenous models, elastic constants (E and v) for the zones were set to 75 GPa and 0.25, respectively. The emergent specimen-scale Young's modulus is known to depend on the contact normal (jkn) and shear (jks) stiffness, while the Poisson's ratio is related to their ratio [52,45]. In order to simplify the calibration process, the ratio was set to 1.5 (within the range prescribed by Fabjan et al. [33] and identical to that used by Farahmand and Diederichs [35]) and the j_{kn} was varied until the Young's modulus and Poisson's ratio matched those reported in Section 2. For the heterogeneous models, a similar approach was taken, with the exception that the blocks were assigned values of E and v from Bass [9] based on their mineral composition (see Table 2). Each mineral block type or mineral-mineral contact type had consistent properties across the entire model (i.e. no randomized distribution was considered within a mineral or mineral-mineral contact type).

(b) The CI threshold and the Brazilian tensile strength are largely dependent on the tensile strength of the block contacts [52,33,98]. The contact strength was varied until a reasonable match with CI and tensile strength values was attained.

(c) The contact cohesions and friction angles affect the CD, macroscopic cohesion and friction angle, and, consequently the unconfined

Table 2
Elastic modulus, Poisson's ratio and density of common minerals in granite (from [9]).

Mineral	Young's Modulus (GPa)	Poisson's Ratio (ν)	Density (g/cc)
Quartz	94.5	0.08	2.65
Plagioclase	88.1	0.26	2.63[a]
Biotite	33.8	0.36	3.05

[a] From Mavko et al. [66].

and confined peak strengths. Based on parametric studies conducted as a part of the calibration process, it was found that the contact cohesion had a greater impact on the sample cohesion, while the contact friction significantly affected the sample friction angle. These findings are consistent with those of Wang and Cai [98]. A best-fit combination of friction angle and cohesion was ultimately chosen from the parametric study.

(d) To simplify the calibration of the contact properties in the heterogeneous models, the properties from Farahmand and Diederichs [35] were selected as a baseline, followed by systematic modifications. Some rules were followed during the manual back-analysis process: (i) Quartz-Quartz (QQ) contacts were assigned higher strength properties than Plagioclase-Plagioclase (PP) contacts, followed by Biotite-Biotite (BB). All bi-minerallic contacts were assigned lower strengths, with QB and PB lower than QP due to the softer biotite association. (ii) The residual contact friction angle was kept constant at 5°, as an increase in residual contact friction angle over 10° resulted in very high triaxial test peak strengths. (iii) The residual cohesion and tensile strength for all contacts were zero.

(e) In the inelastic models, the calibrated contact properties from their elastic counterparts were used as an initial set of parameters. Iterative modifications to the contact and zone strength parameters were ultimately required in order to match the peak strengths for all confining stresses. Typically, the inelastic properties had a minimal effect on the model behavior at low confinement, but their influence increased at higher confinements.

The best parameter set reported for each model type is based on two assumptions. First, if during model calibration, a particular type of model (or complexity level) was found incapable of reproducing all the laboratory-derived attributes, then a logical subset was chosen based on an understanding of the rock damage process. For example, the homogenous, elastic model could not simultaneously capture the peak strengths under low and high confinement. Since elastic blocks neglect any grain damage and given that intra-granular fracturing is an important failure mechanism under high confinements, we chose to replicate the unconfined and low-confinement attributes while allowing disagreement with the high confinement attributes. Secondly, the entire calibration was performed using a single block geometry. The effect of block arrangement on the model results is beyond the scope of this study.

CI and CD in BBMs are commonly identified as the points of tensile crack and shear crack acceleration, respectively [45,71,35]. A review of existing literature revealed that there is no standardized method for selecting such acceleration points. To develop a method that can be used to identify the CI and CD from the crack curves consistently, the % of tensile and shear cracks normalized to the total number of tensile and shear cracks at the onset of residual strength was compared to the CI and CD determined from the ITLS and non-linearity of the axial stress-strain curves in the models, respectively. The purpose of normalizing to the total number of cracks at residual stress level rather than to the total number of contacts was to amplify any change in slope in the crack curves. An example of the normalized tensile and shear crack curves for the heterogeneous, inelastic model is shown in Fig. 4.

Interestingly, the CI from the ITLS and the CD from the non-linearity of the BBM axial stress-strain curves coincided with the point of intersection of the two initial linear segments of the tensile and shear crack curves. The linear segments and point of intersections are shown with black broken lines and red circles in Fig. 4. Since the same trend was observed in all the model types, this methodology was selected for determining CI and CD in this study.

In the UCS and triaxial models, the stresses were calculated as a sum of reaction forces along the top edge of the model, divided by the specimen width. To ensure that the models were at a pseudo-static condition, average vertical zone stresses in three domains that are 40 mm high and 55 mm wide and spanning from the model bottom to the top were also tracked during the simulations and care was taken to ensure that these three curves coincided with the stress determined from the reaction forces. Vertical and lateral strains were computed based on the location of all gridpoints and 11 pairs of gridpoints along the shorter and longer edges of the model, respectively. In the BTS model, the sum of reaction forces (P) along the top of the platen was converted into tensile stress per the equation $\sigma_t = 2P/\pi Dt$, where D is the diameter and t is the thickness of the model (1 unit here). All monitoring was done using user-defined FISH functions executed once every 1000 solution steps.

Rocks loaded under confined conditions show reduced dilatancy due to suppression of brittle extensile fractures. This phenomenon has been qualitatively explored in previous BBM studies using volumetric strain plots [72,35,57]. An alternative approach, based on the determination of peak dilation angles, is employed here which allows for a more quantitative comparison with the laboratory data. A brief description of the approach is presented below. More details can be found in Walton and Diederichs [94].

The macroscopic dilatancy of a specimen can be expressed in terms of the dilation angle (ψ) and is related to the maximum ($\dot{\epsilon}_1^p$)and minimum ($\dot{\epsilon}_3^p$) strain increments as [92]:

$$\sin(\psi) = \frac{\dot{\epsilon}_1^p + 2\,\dot{\epsilon}_3^p}{2\,\dot{\epsilon}_3^p - \dot{\epsilon}_1^p} \tag{3}$$

Several studies [2,106,94]have found the dilation angle to be a function of plastic shear strain (γ^p) and confining stress (σ_3). The plastic shear strain parameter quantifies damage to a rock specimen and can be determined from internal variables as:

$$\gamma^p = \epsilon_1^p - \epsilon_3^p \tag{4}$$

where ϵ_1^p and ϵ_3^p are maximum and minimum inelastic strains, respectively. Determination of the instantaneous dilation angle require estimation of the axial and lateral (or maximum and minimum) plastic strain increments. Walton and Diederichs [94] developed a new approach (Eqs. (5) and (6)) that uses the concepts of elasticity theory and the definition of CI and CD in Diederichs and Martin [27] for calculating these quantities. The equations essentially subtract the elastic component of the total strain, along with axial plastic and lateral plastic strains at CD and CI, to obtain ϵ_1^p and ϵ_3^p respectively.

$$\epsilon_1^p = \epsilon_1 - \epsilon_{1(CD)} - \frac{\sigma_1 - CD}{E} \tag{5}$$

$$\epsilon_3^p = \epsilon_3 - \epsilon_{3(CI)} + \nu\frac{\sigma_1 - CI}{E} \tag{6}$$

Lastly, to satisfy the condition of yield at CD, i.e. $\gamma^p = 0$, the plastic shear strain obtained from Eq. (4) needs to be shifted by γ_{CD}^p. The maximum value of instantaneous dilation angle is the peak dilation angle for each specimen. The peak dilation angles for 10 MPa, 20 MPa, 40 MPa and 60 MPa BBMs, normalized to the peak dilation angle for UCS, were ultimately determined and compared to the corresponding values from laboratory testing. To provide for a better understanding of how the volumetric characteristics of the models evolve with loading, volumetric strain – axial strain curves have also been presented for all the model cases.

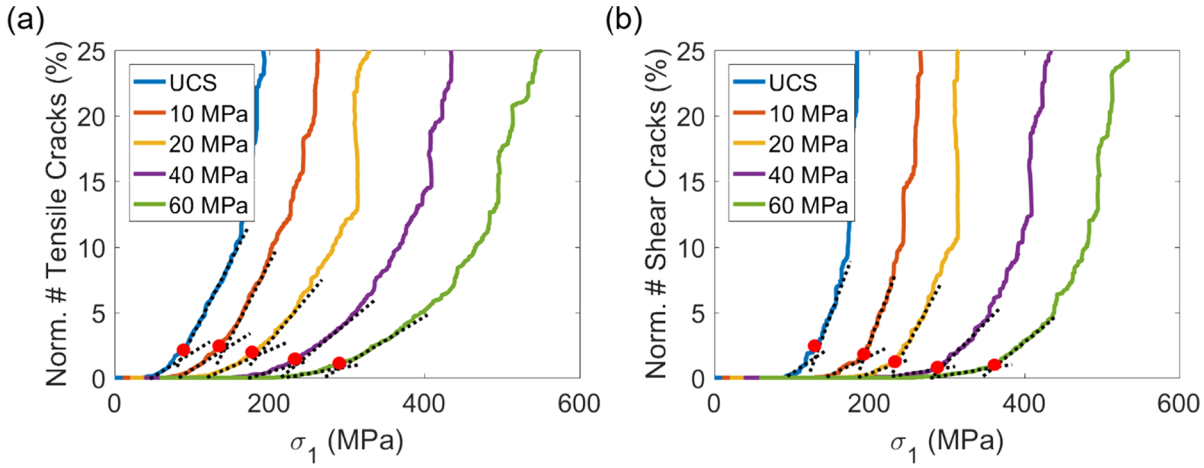

Fig. 4. Methodology for identifying (a) CI, and, (b) CD, from the normalized number of tensile and shear cracks in the model. These graphs correspond to the heterogeneous, inelastic BBMs (Section 5.4).

5. Results

In this section, the results corresponding to best-fit parameter sets are presented in order of increasing model complexity. Some alternative parameter combinations and their results are also discussed. The parameters presented in any given section represent one of the many similar parameter sets that fit the laboratory data equally well. During the model calibration stage, we found that typically a range for each parameter rather than a unique parameter set is obtained from back-analysis. While the values reported here are chosen from the middle of this range, selection of other similar parameter combinations would not have affected the conclusions of this study.

5.1. Homogenous, elastic BBM

Fig. 5(a–d) shows the model-predicted stress-strain curves for UCS and triaxial simulations, peak strengths, CI and CD, respectively. The corresponding input parameters are listed in Table 3. Elastic BBMs are known to exhibit prolonged pre-peak hardening under confinement [89,6,99], and such a behavior was observed in the models. Following the onset of yield (axial strain non-linearity), the model behaved in a brittle fashion only for the UCS condition. The actual stress-strain curves for Creighton granite were brittle even under a confining stress of 60 MPa. Clearly, the macroscopic behavior of the BBM is inconsistent with that of the real rock.

In spite of the unrealistic hardening in the stress-strain curve, the peak strengths up to σ_3 = 20 MPa matched the laboratory data. Interestingly enough, this range of confinement, i.e. 0–10% UCS, lines up perfectly with the previous attempts to capture triaxial strengths using homogenous, elastic BBMs [89]. For σ_3 = 40 MPa and σ_3 = 60 MPa, the peak strengths are significantly overestimated and this can be explained by the lack of grain-fracturing capabilities in these models. For the Brazilian test, the corrected tensile strength was 8.6 MPa, which is only 0.4 MPa less than the average tensile strength of Creighton granite.

Fracture initiation in homogenous BBMs is governed largely by point loads (wedging) generated during grain translation and rotation. Since the block structure is compact, a considerable amount of axial straining is required to generate adequate tensile stress within the model. Due to this, the onset of microfracturing is somewhat delayed. As shown in Fig. 5c, the discrepancy between the model-predicted CI and the laboratory data increases with an increase in confinement. While the CI for the unconfined condition is within the range of laboratory data, further reduction was not possible without increasing the data-model misfit in tensile strength. This is because CI is controlled entirely by the contact tensile strength [52,33,98], which also happens to affect the Brazilian tensile strength.

The CD values predicted by the BBM are close to the upper bound of the laboratory data for σ_3 = 0–20 MPa confinement and are clearly too high in the 40 and 60 MPa triaxial models. The lack of pre-peak hardening under unconfined conditions, manifesting in a larger CD value, can also be observed in other UDEC-BBM studies [33,89]. In an attempt to lower the CD for the UCS model, a separate sensitivity analysis was conducted. It was found that instead of a softening-type contact (i.e. simultaneous degradation of friction and cohesion upon failure), a CWFS-type contact (cohesion degraded but friction mobilized post failure) performed better in allowing greater pre-peak hardening prior to failure. The softening-type and CWFS-type contacts are illustrated using schematic diagrams in the Appendix. In the “CWFS contact” type model, the contact cohesion degraded from 100 MPa to 0 MPa and the friction mobilized from 0° to 52°. While this model type could also capture the tensile strength fairly well (8.1 MPa), the triaxial strengths were far too high (Fig. 5b). A similar contact representation was used by Ghazvinian et al. [45]. In light of the current results and the fact that Ghazvinian et al. [45] only performed calibration for unconfined conditions, it can be concluded that a CWFS-type contact is not suitable for simulating confined rock behavior.

In the softening contact-type model, the CI threshold crossed the CD threshold around a confining stress of 20 MPa. When confining stresses are high in BBMs, local tensile stresses are naturally suppressed, which forces the micro-fractures to initiate in a shear mode. Only when the blocks slide past one another and wedging is enhanced do the contacts start to fail in tension. This sequence of microfracturing does not occur in reality and highlights the role that stiffness heterogeneity plays in inducing damage in rocks.

A CI threshold larger than CD threshold is physically not meaningful and has not been reported in the literature for any crystalline rocks. Since the definitions of CI and CD do not hold for these higher confinement BBMs, the peak dilation angle comparison is not presented. Fig. 5e shows the volumetric strain-axial strain plot for the homogenous elastic BBMs. The volumetric expansion as well as the rate of dilation decreased noticeably with confinement. This is in keeping with how rocks respond under compression [104,106,4] and is consistent with other BBM studies as well [72,35,57].

5.2. Homogenous, inelastic BBM

Intra-granular fracturing can be implicitly modeled in UDEC-BBM by allowing the zones to yield inelastically according to a strain-softening constitutive model. The abundance of such fractures in rocks

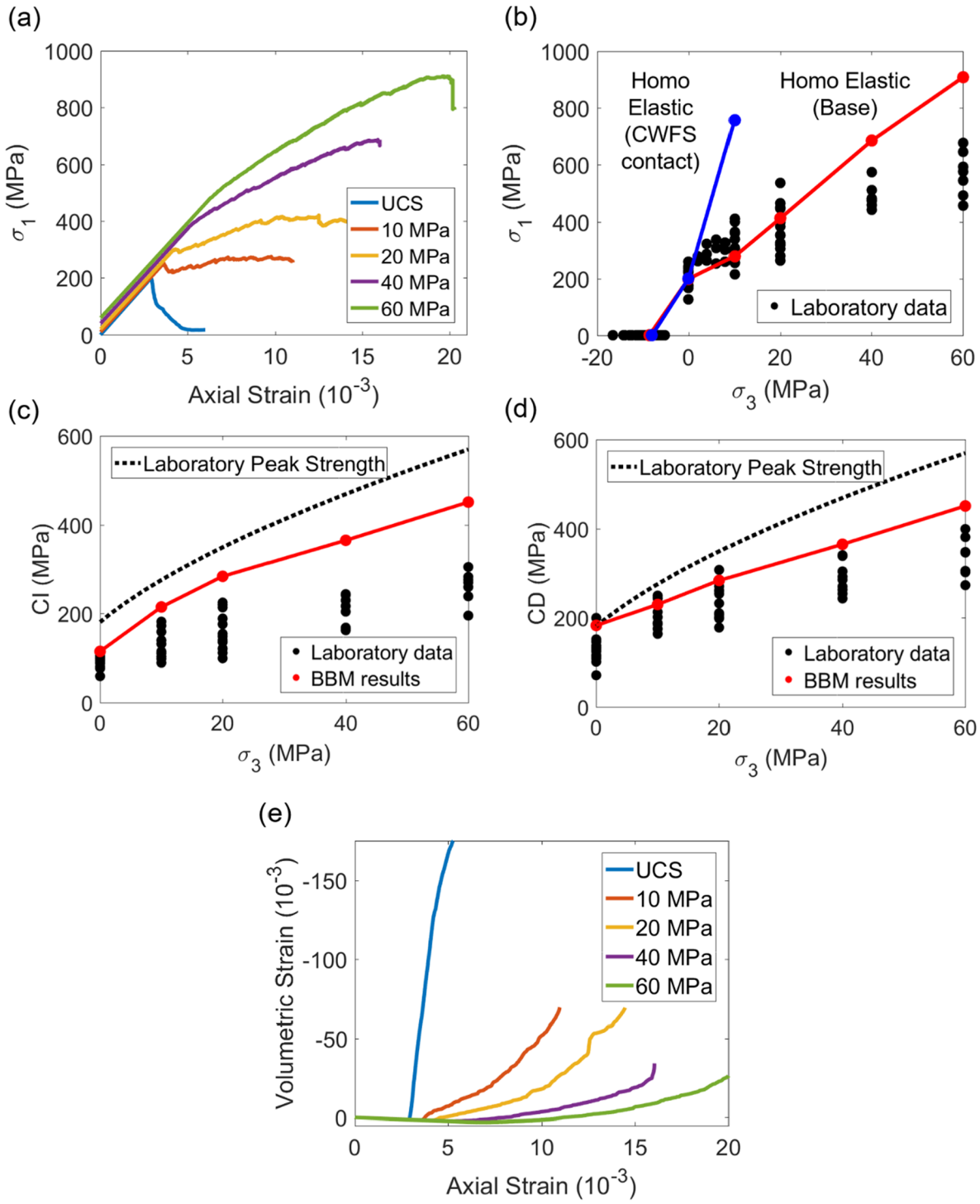

Fig. 5. (a) Stress-strain curves for 0–60 MPa confinement, (b) Model strengths for Base and 'CWFS contact' model in σ_1–σ_3 space. (c) CI Thresholds, (d) CD Thresholds, and, (e) Volumetric strain versus axial strain.

Table 3
Input parameters for homogenous, elastic BBM.

Contact normal stiffness (j kn; GPa/m)	Contact cohesion (j coh; MPa)	Contact friction (j fric; deg)	Contact residual cohesion (j rcoh; MPa)	Contact residual friction (j rfric; deg)	Contact tensile strength (j tens; MPa)
230,000	66	43	0	35	17

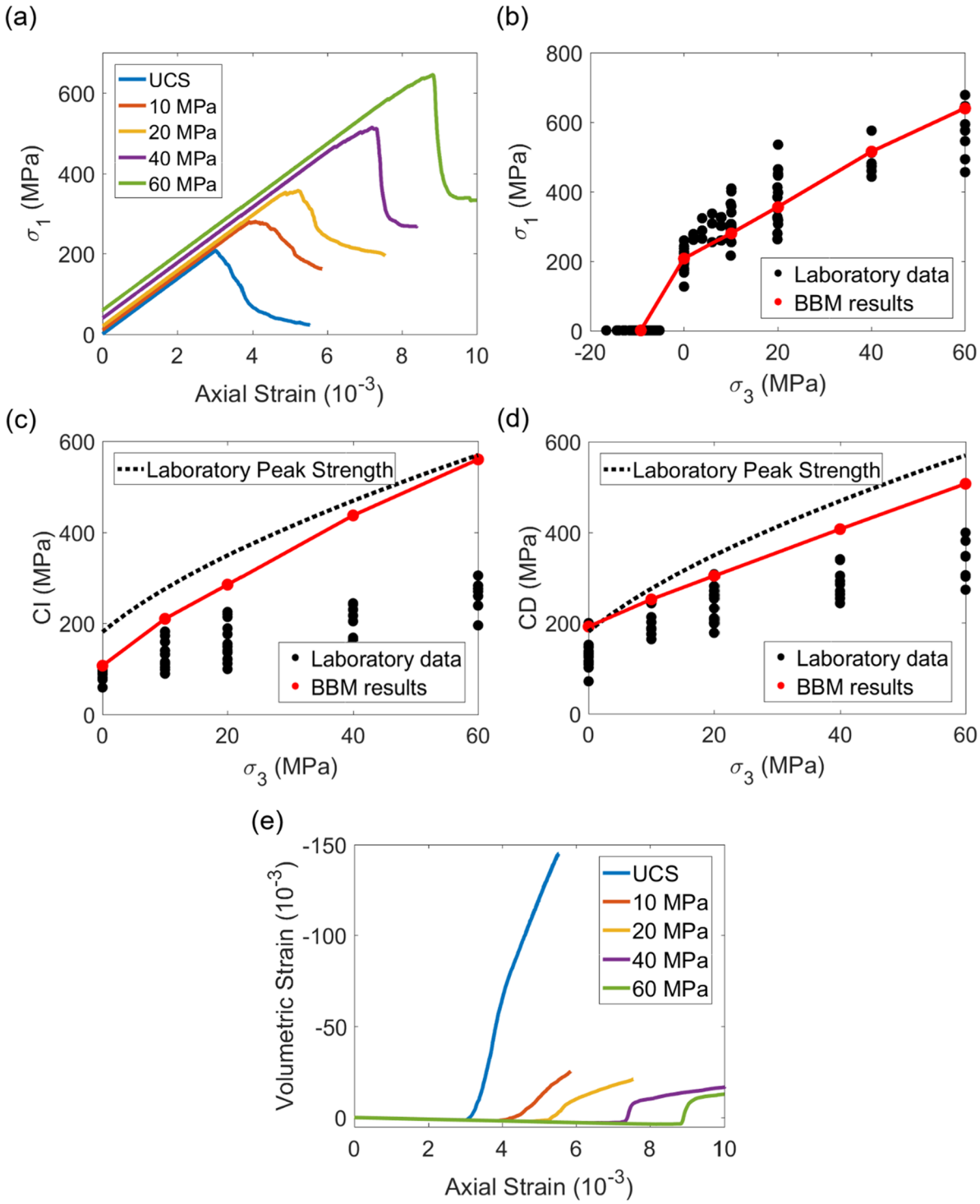

Fig. 6. (a) Stress-strain curves for 0–60 MPa confinement, (b) Model strengths in σ_1–σ_3 space. (c) CI Thresholds, and, (d) CD Thresholds, and (e) Volumetric strain versus axial strain.

tested under confinement has been confirmed in the past using image analysis techniques [69,88,90,46]. Despite its importance, the majority of previous BBM studies have only considered elastic blocks in their simulations.

The incorporation of an inelastic constitutive model in the zones undoubtedly improves the phenomenological capability of the model but it also increases the number of input parameters by a factor of two. The additional (zone) parameters are the peak and residual cohesion, peak and residual friction angle, peak and residual tensile strength, dilation angle and the plastic strain over which the peak values are degraded to their residual counterparts (assumed here to be identical for all parameters). The zone strength parameters should lie within a reasonable range as expected for actual mineral grains, although these values are not directly measureable in laboratory and are neither well constrained in literature. Hence, the input parameters reported are based solely on the ability of the models to match the laboratory attributes, with some intermediate reliability checks against the values used by Noorani and Cai [72] and Wang and Cai [99].

Fig. 6(a–d) shows the stress-strain curves, peak strengths, CI and CD from the best-fit model. The relevant input parameters are listed in

Table 4
Input parameters for homogenous, inelastic BBM; ε_{ps} is the plastic strain over which the parameters degraded from peak to residual values.

Contact properties			Zone properties					
j kn (GPa/m)	j coh (MPa)	j fric (deg)	Cohesion (MPa)		Friction angle (°)		Tens strength (MPa)	
			Peak (c_{peak})	Residual (c_{res})	Peak (ϕ_{peak})	Residual (ϕ_{res})	Peak ($\sigma_{t,peak}$)	Residual ($\sigma_{t,res}$)
230,000	65	50	100	30	55	30	38	0
j rfric (deg)	j tens (MPa)	j rtens &j rcoh	ε_{ps}		Peak dilation angle (ψ_{peak} – °)		Residual dilation angle (ψ_{peak} – °)	
32.5	15	0	0.03		30		10	

Table 4. The most prominent difference with respect to elastic BBMs is the absence of significant pre-peak hardening in the stress-strain curves (Fig. 6a); a similar observation was made by Wang and Cai [99]. The overall shape is fairly consistent with the laboratory curves for Creighton granite. Surprisingly, the post-peak drop modulus values in the σ_3 = 40 MPa and σ_3 = 60 MPa models were larger than the UCS, 10 MPa and 20 MPa models and this trend is not consistent with true rock behavior [3,4,16]. The disagreement is likely related to the failure being dominated by the inelastic damage of the zones rather than by opening of block contacts.

A gradual increase in the post-peak drop modulus can also be observed in the stress-strain curves of Wang and Cai [99]. Intuitively, if the drop modulus is dependent on the rate of degradation of the zone strength envelope, then a larger plastic shear strain lag should result in a slower decay in stress. Increasing the ε_{ps} indeed resulted in a lower drop modulus, but it also increased the σ_3 = 40 MPa and σ_3 = 60 MPa peak strengths significantly. The zone strength parameters could not be lowered to counterbalance this strength rise, because it led to large mismatch in the peak strengths for the UCS, σ_3 = 10 MPa and σ_3 = 20 MPa models.

The calibrated BBM could capture the peak strengths for the entire range of confining stress tested (Fig. 6b). For this set of parameters, the tensile strength was 9.2 MPa. As can be seen in Fig. 6c, CI was overestimated for all the triaxial models. Under unconfined conditions, the value was close to the upper limit of the laboratory data. Recalling that the homogenous, elastic BBM also behaved in a similar fashion, it could be inferred that homogenous models are not capable of capturing the true pre-peak micro-damage process in its entirety. CI values were not reported by Noorani and Cai [72] and were only reported for UCS conditions by Wang and Cai [99].

The CD thresholds only approximately matched laboratory values in the UCS, σ_3 = 10 MPa and σ_3 = 20 MPa models, but are overestimated in the σ_3 = 40 MPa and σ_3 = 60 MPa models (Fig. 6d). The lack of pre-peak hardening in the UCS model does not agree with the results from Noorani and Cai [72], who reported a CD of 71% UCS. The key difference in model parameters that is believed to have caused this effect is that Noorani and Cai [72] opted for the same zone tensile strength as those of the block contacts (12.1 MPa), on the grounds that intragranular fracturing is prevalent in UCS and contributes to the large dilation commonly seen in laboratory tests. The plot of yielded zones in Noorani and Cai [72] further indicates that almost all zones in the model had failed in tension. Although it is true that UCS tests on granitic rocks typically involve large volumetric strains, there is no evidence in literature that the damage is pervasive across the entire volume of the specimen nor that the damage is dominantly intragranular in nature [32,60]. It is also counterintuitive for an intact mineral grain to have the same tensile strength as that of a contact, as contacts should be inherent points of weakness within the grain structure.

The distribution of damaged contacts in the triaxial models were markedly localized. Part of the reason is that as the zones started to contribute more towards the failure of the specimen, less contacts were involved and block motions were arrested. The zones, because of their continuum formulation, do not possess the same dilating capacity as the block contacts. This also explains why the volumetric strain magnitudes are lower than in the elastic models (compare Fig. 6e and Fig. 5e).

5.3. Heterogeneous, elastic BBM

The contribution of microstructural heterogeneity towards the progressive damage in rocks has already been discussed. Based on the results so far, one can understand that it is not possible to reproduce tensile microcracking under confined conditions with a homogenous block assumption. Farahmand and Diederichs [35] showed that CI under unconfined and low confinement conditions can be realistically captured using elastic, heterogeneous models. To ascertain whether heterogeneous BBMs have the capability of predicting damage initiation under even higher confinement, 3 sets of elastic properties, corresponding to Quartz, Plagioclase and Biotite mineral grains, were assigned to the block model. In addition to the elastic parameters (Table 2), the models require 6 sets of contact properties. It is apparent that the degree of non-uniqueness is much higher in these models, with over 40 input parameters. Table 5 lists the final set of input parameters. This set of model is termed as 'Base', and the associated results are presented below.

Fig. 7(a–d; Base) shows the stress-strain curves, model strengths in σ_1–σ_3 space, CI thresholds and CD thresholds, respectively. Similar to the homogenous, elastic BBMs, the models exhibited enhanced strain hardening prior to failure (Fig. 7a). The UCS and triaxial strengths up to σ_3 = 20 MPa are well captured, but the high confinement strengths are over-estimated. The most prominent difference with respect to the homogenous models is the ability to match the CI and CD for the entire range of confining stress (Fig. 7c and d).

In order to better understand the effect of microstructural heterogeneity on stress localization in the unconfined models, the minor principal stresses (σ_3) were extracted from the elastic, homogenous and elastic, heterogeneous BBMs at an average axial stress of 89 MPa, which is the value of CI for the unconfined heterogeneous elastic BBM (see Fig. 8). The goal is to compare the range of tensile stresses developed within the two models at the same loading stage. As can be seen, much larger tensile stresses localize within the heterogeneous model in comparison to its homogenous counterpart. Tensile stresses over ~20 MPa are also highly localized in the model. The difference in the extent of stress perturbation explains why the CI could be represented in the unconfined and the triaxial models (similar reasoning), even though the contact micro-tensile strengths assigned are much larger than those in the homogenous BBMs.

Table 5
Contact input parameters for heterogeneous, elastic BBM (Base).

Contacts	j kn (GPa/m)	j coh (MPa)	j fric (deg.)	j tens (MPa)
Q-Q	280,000	130	65	31
P-P	250,000	112	63	31
B-B	130,000	98	60	22
Q-P	230,000	90	60	24
Q-B	230,000	67	55	21
P-B	230,000	64	55	20

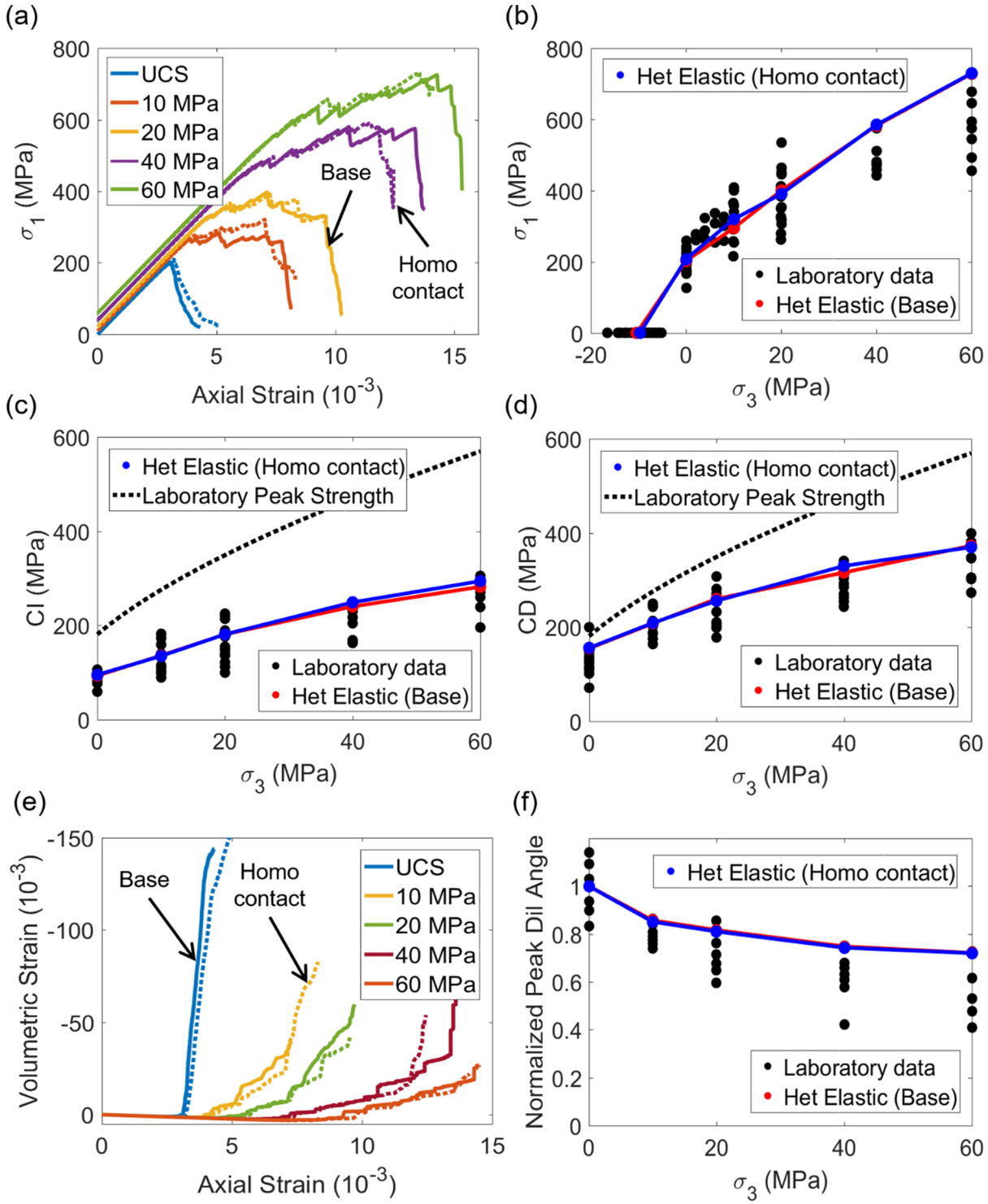

Fig. 7. (a) Stress-strain curves for 0–60 MPa confinement, (b) Model strengths in σ_1–σ_3 space, (c) CI Thresholds, (d) CD Thresholds, (e) Volumetric strain – axial strain, and, (f) Normalized peak dilation angle versus confinement plots for the 'Base' and 'Homo contact' models.

It appears that the early initiation of micro-cracks eventually affects its subsequent growth and interaction. A closer look at the crack development modes revealed that even in the σ_3 = 60 MPa model, tensile cracks dominated up to slightly beyond the CD threshold. The abundance of tensile cracks at advanced stages of loading indicates the continued role that microstructural heterogeneity plays in controlling the fracture evolution process.

After peak strength, all models exhibited instantaneous drops in the axial stress before completely losing their load carrying capacity. The post-peak drop modulus values are high and are not consistent with the laboratory test data. A similar behavior can be noted in the stress-strain curves from Chen et al. [17]. It seems that the lack of zone inelasticity is responsible for the over-prediction of the σ_3 = 40 MPa and σ_3 = 60 MPa strengths as well as the mismatch in the post-peak behavior.

The volumetric strains and the normalized peak dilation angles were determined from the axial stress – strain and axial stress – lateral strain curves (see Fig. 7e and f). The decreasing trend in the laboratory data in

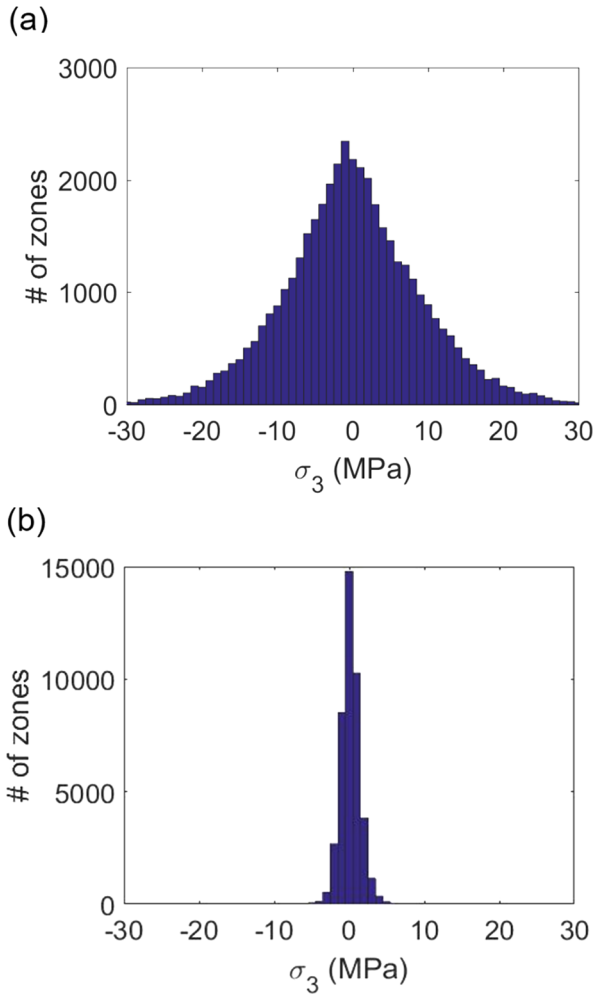

Fig. 8. Distribution of confinement in model zones at σ_1 = 89 MPa in (a) heterogeneous, elastic model, and, (b) homogenous, elastic model.

Fig. 7f signifies a change in the mode of fracture formation from highly dilatant extensile (axial) cracking to medium-low dilation shear (oblique) cracking as noted by Walton and Diederichs [94]. This confinement-dependent dilatancy phenomenon is well captured by the models. The data-model discrepancy at higher confinements (Fig. 7f) can be attributed to the lack of intra-grain damage (i.e. elastic zones) and the greater ability of block contacts to dilate in comparison to the zones.

All of the aforementioned results correspond to BBMs that had different stiffnesses and strengths assigned to the block contacts. There is another contact representation in literature that is characterized by different contact stiffnesses (i.e. j_{kn}, j_{ks}) but similar contact strengths [54,71,75]. This is a major simplification relative to the completely heterogeneous model, and it reduces the number of input parameters appreciably. From a mechanistic standpoint, the rationale for the use of different stiffnesses yet similar strengths is somewhat ambiguous; one would expect the strengths as well as the stiffnesses to be different for different mineral contact associations. The assumption might be based on the concept that different stiffnesses would induce different amounts of stress at the contacts. If the same logic is followed, then one can argue that elastic zone mismatch will generate enough stress heterogeneity and the use of uniform contact properties (strength and stiffness) in a BBM might be a sufficient approximation for practical purposes.

Surprisingly enough, when a homogenous contact BBM with j_{kn} = 22500 GPa/m, j_{kn}/j_{ks} = 1.5, j_{coh} = 89 MPa, j_{fric} = 57.5° and j_{tens} = 25 MPa (termed as 'Homo contact') was run, it was found to be capable of reproducing all the laboratory attributes equally well (Fig. 7). Only a slight discrepancy was noted between the CI predicted by the Base and 'Homo contact' models at higher confinements. This could be attributed either to the reduced phenomenological capability of the 'Homo contact' models (i.e. no contact heterogeneity) or it could be a limitation of the calibration process itself. In any case, it appears that the consideration of elastic block heterogeneity is far more important than contact heterogeneity towards capturing the micro-damage process.

5.4. Heterogeneous, inelastic model

Based on the results so far, two conclusions can be drawn: (1) Microstructural stiffness heterogeneity is necessary for reproducing the confined CI and CD; (2) Allowing intra-granular fracturing via zone yield is critical to allow accurate representation of confined peak and post-peak behavior. A BBM with both these characteristics should be able to match all the laboratory derived attributes. The authors are unaware of any previous studies that have considered block and contact heterogeneity and zone inelasticity simultaneously. The reason is likely the difficulty of calibrating complex models that have over 60 input parameters to constrain. Here we matched 22 different laboratory attributes (5 peak strengths, tensile strength, 2 elastic constants, 5 CIs, 5 CDs and 4 normalized dilation angle values) and qualitatively compared the post-peak behavior with those from the laboratory. Although there are many more model inputs than calibration targets (~3 times), some of the model input parameters (E, ν of minerals) were either constrained from literature or were not varied (residual friction angle, cohesion and tensile strength of contacts, etc.). The total number of parameters that were constrained was only 38, which lowers the ratio of input parameters to calibration targets to 38/22 = 1.73. This value is comparable to prior studies conducted using UDEC-BBM. Additionally, even for parameters that were varied as part of the calibration process, many could be bounded within a limited range of physically reasonable values. For example, the friction angle and tensile strength for the contacts was varied in the range of 40°-65° and 10–35 MPa, respectively [15,35].

Given the approach adopted in this study (gradual increase in complexity with intermediate calibration steps), it was possible to integrate both block and contact heterogeneity and zone inelasticity in a BBM and constrain it with modest calibration efforts. Specifically, the contact properties listed in Table 5 and the strain softening parameters in Table 4 were selected as baselines and then modified systematically until the calibration targets were met. In order to limit the degree of model non-uniqueness, only one set of strain-softening zone parameters was assigned to the entire model. The use of three sets of zone strain-softening parameters for the three mineral types may be more physically accurate, but was not considered as the current set of models was able to match all recorded attributes of Creighton Granite. Table 6 and 7 lists the best-fit input parameters.

The stress-strain curves obtained are relatively brittle, with modest pre-peak hardening (Fig. 9a) and are generally consistent with the laboratory data. During the model calibration phase, it was found that a high ε_{ps} in the strain-softening model was required to obtain a consistent reduction in post-peak modulus with confinement. This value is

Table 6
Contact input parameters for heterogeneous, inelastic BBM.

Contacts	j kn (GPa/m)	j coh (MPa)	j fric (deg.)	j tens (MPa)
Q-Q	280,000	105	63	28
P-P	250,000	95	61	27
B-B	130,000	80	58	20
Q-P	230,000	90	53	21
Q-B	230,000	60	51	18
P-B	230,000	60	51	18

Table 7
Zone input parameters for heterogeneous, inelastic BBM.

Cohesion (MPa)		Friction angle (deg)		Tensile strength (MPa)		Dilation angle (deg)		ε_{ps}
Peak (c_{peak})	Residual(c_{res})	Peak (φ_{peak})	Residual(ϕ_{res})	Peak ($\sigma_{t,peak}$)	Residual($\sigma_{t,res}$)	Peak	Residual	0.1
118.5	48.5	65	47.8	51.5	0	15	10	

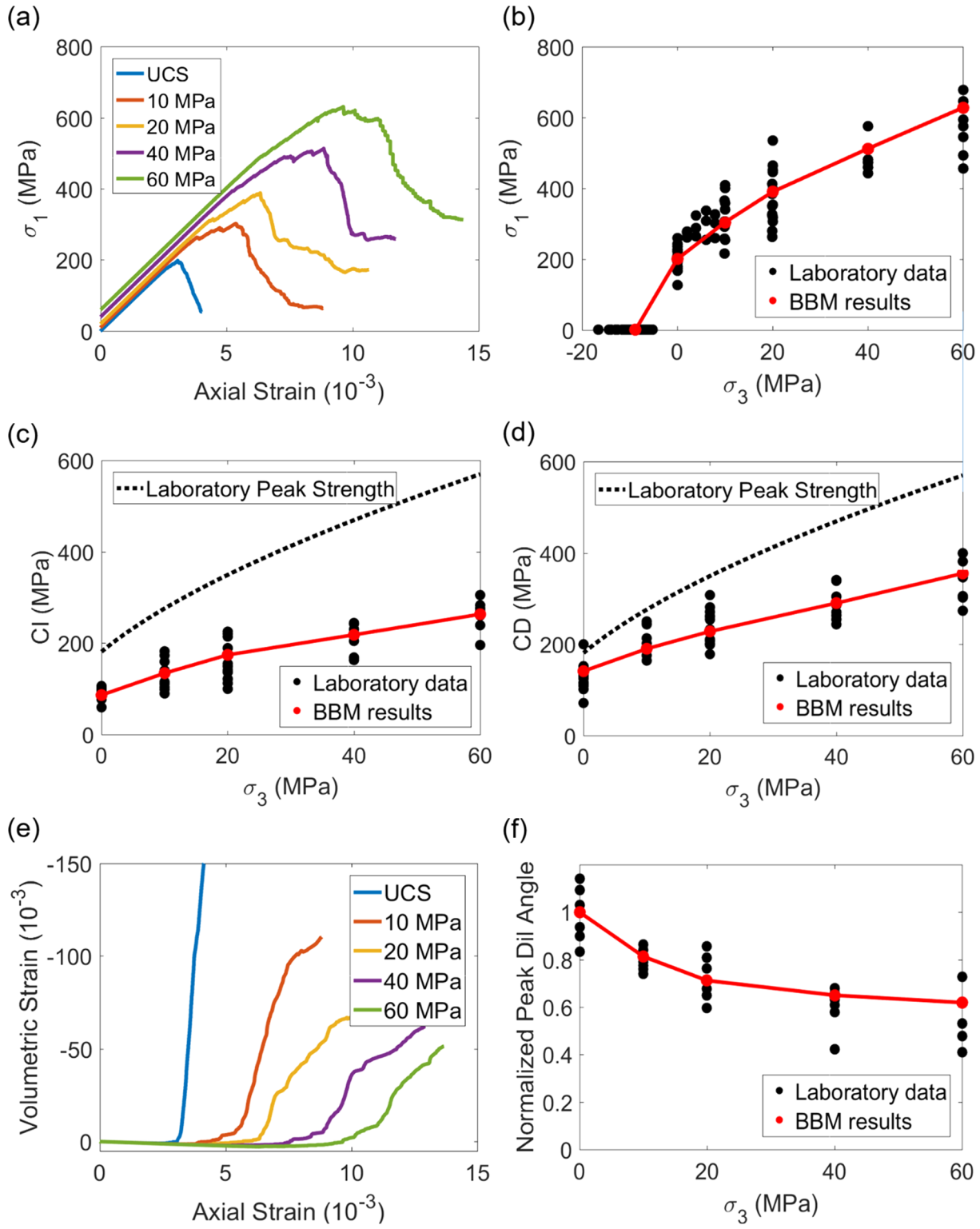

Fig. 9. (a) Stress-strain curves for 0–60 MPa confinement, (b) Model strengths in σ_1- σ_3 space. (c) CI Thresholds, (d) CD Thresholds, (e) Volumetric strain – axial strain, and, (f) Normalized peak dilation angle versus confinement.

much larger than those used by Noorani and Cai [72] and Wang and Cai [99]; however, ε_{ps} is a zone size-dependent parameter and a direct comparison is therefore not possible. A large ε_{ps}implies a slower drop from the peak to the residual stress level and could be interpreted to represent the progressive aggregation of micro-fractures within a zone-sized region in a mineral grain before its strength is reduced.

Fig. 9b shows the peak strengths in σ_1-σ_3 space. To the best of our knowledge, this is the first time that the non-linear trend of the strength envelope has been clearly replicated using UDEC-BBM. The CI and CD thresholds were also reproduced in these models (Fig. 9c and d). The tensile strength was 8.8 MPa, which is only 0.2 MPa lower than the average tensile strength of Creighton granite. Failure in the BTS specimen (also in the previous models) occurred through the formation of a diametrical crack between the two platens. Once the peak tensile strength was attained, the stress–strain curve dropped in a brittle fashion. These results are similar to those reported by Farahmand and Diederichs [35], Gao et al. [39] and Park et al. [75]. The trend of normalized peak dilation angle as well as the volume change in the specimen was also consistent with the laboratory data (Fig. 9e and f), and highlights the well-calibrated nature of the BBM.

5.5. Crack types and zone yields in different BBMs

The percentages of damaged contacts and yielded zones at peak strength for the different models are presented in Fig. 10. The contacts have been further subdivided on the basis of whether they fractured in shear or in tension. While it is possible to compare the number of intra-granular and grain-boundary fractures in PFC-GBMs, a direct comparison in this case is not physically meaningful. In PFC-GBM, the breakage of one parallel bond at the disc contact can be correlated to one fracture in real rock. In UDEC-BBM, the yield of one zone does not necessarily relate to a single fracture; rather it relates to an aggregate of fractures, and the number of fractures within this aggregate at an instant defines the position of the zone strength envelope between the peak and the residual. In other words, an increase in plastic shear strain implies a physical increase in the concentration of intra-granular fractures. Since this phenomenon is abstract and difficult to quantify, only the % of yielded zones is reported in Fig. 10. The total number of zones and contacts in the models are 42506 and 19333, respectively.

A general drop in the number of tensile cracks and a rise in the number of shear cracks was noted with confinement. A similar change in grain-boundary failure mode from tensile to shear has been reported from other numerical modeling studies by Hofmann et al. [49], Abdelaziz et al. [1], Peng et al. [76] and Li et al. [57]. Interestingly, all the 10 MPa models showed a larger number of tensile grain-boundary cracks at peak strength in comparison to the UCS models. The exact cause for this behavior is not fully understood, but may be related to the fact that triaxial models are confined and require more damage (e.g. hardening) before the peak strength is attained. When the BBM is unconfined, development of a few extensile fractures is sufficient to lose

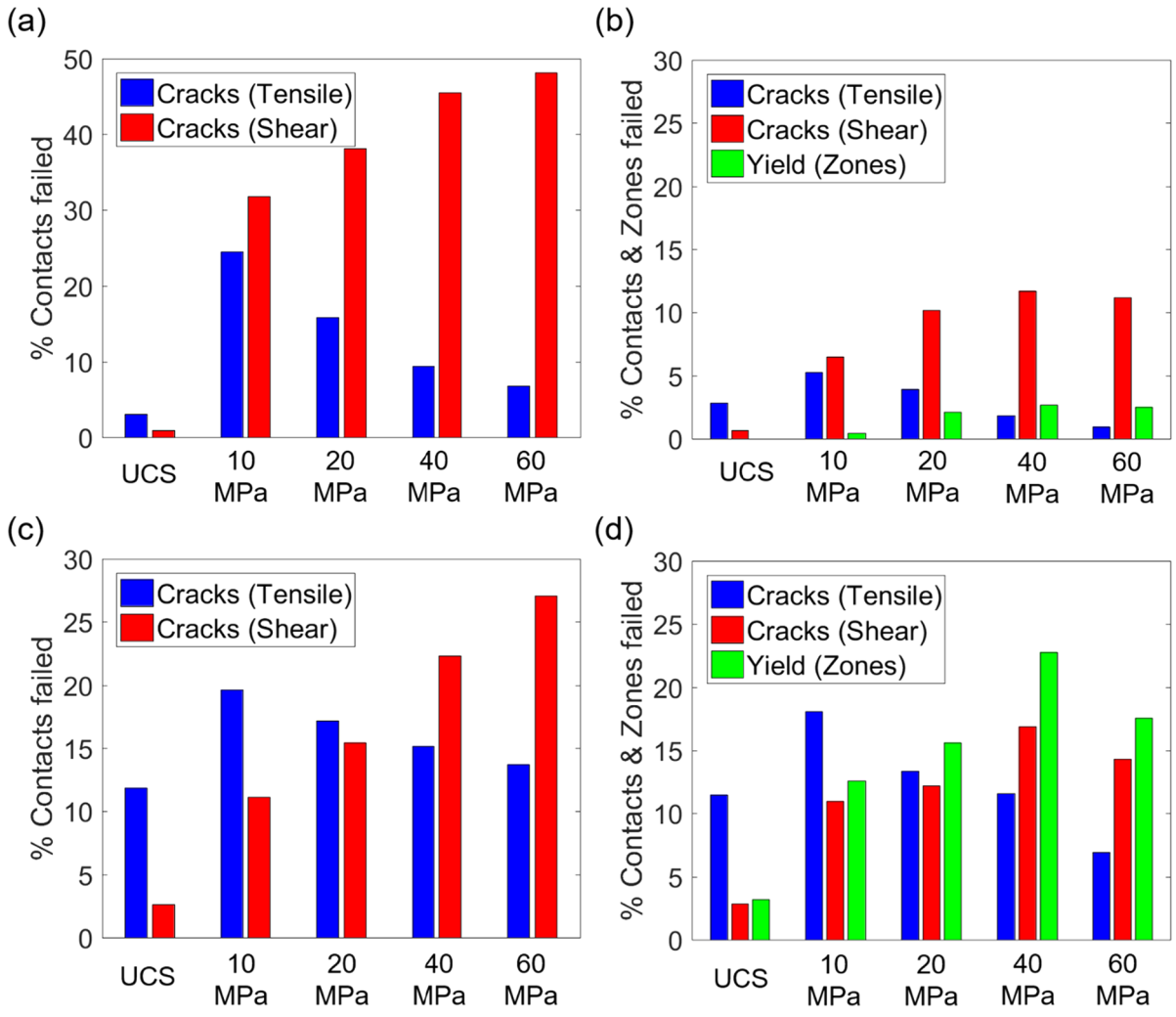

Fig. 10. Cracks and zone yield (in %) for the (a) Homogenous, Elastic BBM, (b) Homogenous, Inelastic BBM, (c) Heterogeneous, Elastic BBM, and, (d) Heterogeneous, Inelastic BBM at respective peak strengths.

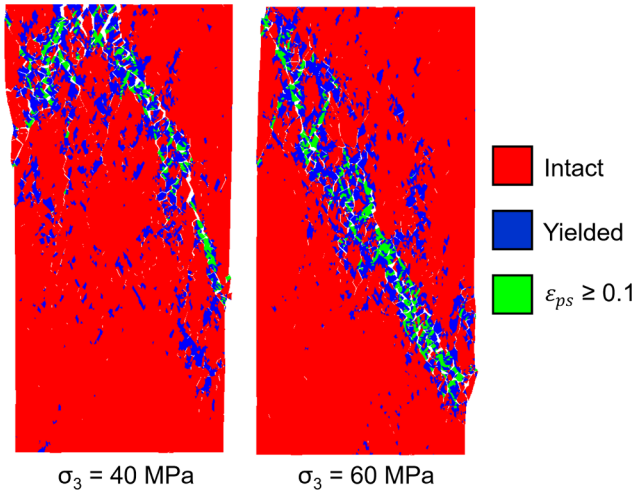

Fig. 11. Contour of yielded zones in the 40 MPa and 60 MPa heterogeneous, inelastic BBM.

its load carrying capacity. This proposition is consistent with previous modeling studies [49,76]and the fact that the cumulative % of shear and tensile cracks in all the confined BBMs are larger than in the unconfined ones.

The role of intra-granular fracturing in controlling the failure of confined BBMs is evident from Fig. 10b and d. The number of yielded zones increased consistently with increase in confinement, barring only the $\sigma_3 = 60$ MPa models. It seems that damage is more localized in the $\sigma_3 = 60$ MPa models and thereby involves a smaller number of zones in the failure process (Fig. 10b and d). This can be verified from plots of yielded zones in the $\sigma_3 = 40$ MPa and $\sigma_3 = 60$ MPa heterogeneous inelastic models, which are shown in Fig. 11. In addition to the localized nature, the damage intensity (ε_{ps}) in the $\sigma_3 = 60$ MPa model was also proportionately larger than in the $\sigma_3 = 40$ MPa model.

The elastic BBMs exhibited greater contact damage than the inelastic models. The involvement of a larger number of contacts is intuitive, as elastic models do not have intra-granular fracturing capability. Lastly, it can be seen that due to lack of stress heterogeneity and appreciable pre-peak hardening, the damage process was extremely localized in the homogenous, inelastic BBMs (Fig. 10b).

6. Discussion

As previously documented in the literature, the homogenous, elastic block models could match the unconfined and low confinement peak strengths from the laboratory, but performed poorly in capturing the confined peak strengths and the microfracture evolution process. Their application should therefore be restricted to studying rock behavior under low confining stresses only. The ability to model the microfracturing process was much enhanced when different mineral blocks were introduced in the BBM. The elastic mismatch played a vital role in inducing initial microcracks as well as subsequent interaction and growth. Like the homogenous BBMs, these models also overestimated the peak strengths at high confinement owing to the lack of grain fracturing capability. Realistic spalling around a circular tunnel was modeled by Farahmand et al. [36] using a scaled-up version of this approach.

Some authors have proposed a modification to the completely heterogeneous BBM representation that has different contact stiffnesses but uniform strengths. In order to isolate the effect of contact heterogeneity relative to that of block stiffness heterogeneity, a supplementary set of models was run with heterogeneous blocks (variable properties by mineral type) but homogenous contact properties (both stiffnesses and strengths). The data-model fit was found to be as good as those in the completely heterogeneous counterpart. It seems that the effect of elastic block heterogeneity is far more pronounced and overshadowed the effect of contact heterogeneity. Given that these BBMs required only one set of contact parameters and were easier to calibrate, modelers might consider employing this semi-heterogeneous representation in future.

The heterogeneous, elastic BBM (with or without contact heterogeneity) managed to capture all the laboratory-derived attributes commonly considered for calibration. Replicating more advanced attributes like peak strength at high confinements, realistic pre-peak hardening, confinement-dependent dilatancy and post-peak modulus required additional phenomenological capability in the form of inelastic zones. The yield of zones within blocks mimics the intra-granular fracturing process, which is known to be an important damage mechanism both under high confining stress and in the post-peak regime. Note that it was important to consider zone inelasticity in conjunction with block heterogeneity to capture all the aforementioned attributes. Block heterogeneity is strongly tied to the initiation and propagation of cracking in BBMs and omitting its effect led to overestimation of CI and CD. The heterogeneous, inelastic BBM could reproduce all the known geomechanical attributes of Creighton granite, and is therefore a reasonable approximation of reality.

The above findings are concisely summarized in Table 8. The authors believe that this table will assist future researchers in selecting a BBM representation that is suitable to a particular problem. When using

Table 8
Capabilities of different BBM representations.

Macroscopic attributes	Homogenous, Elastic	Homogenous, Inelastic	Heterogeneous, Elastic	Heterogeneous, Inelastic
Elastic constants (E, v)	✓	✓	✓	✓
UCS	✓	✓	✓	✓
Tensile strength	✓	✓	x	✓
Low confinement peak strength ($\sigma_3 \leq$ 10% UCS)	✓	✓	✓	✓
High confinement peak strength ($\sigma_3 >$ 10% UCS)	x	✓	x	✓
Unconfined CI	✓	✓	✓	✓
Confined CI	✓ [a]	✓ [a]	✓	✓
Unconfined CD	✓ [a]	✓ [a]	✓	✓
Confined CD	x	x	✓	✓
Pre-peak behavior (confined)	x [b]	✓	x [b]	✓
Post-peak behavior (confined)	x [c]	✓	x [c]	✓
Confinement dependent dilatancy	✓ [d]	✓ [d]	✓	✓

x – cannot match.
[a] Slightly overestimates.
[b] Excessive strain-hardening.
[c] Rapid drop.
[d] Captures qualitative trends only.

this table to decide what constitutes a suitable model representation, one should consider the availability of calibration data as well as the ability of the model to capture the mechanisms relevant to the problem. For example, if BBM is used for studying the fracture evolution in centrally cracked Brazilian discs (CCBD, [15], then a heterogeneous, elastic representation suffices. This is because heterogeneous, elastic BBMs can realistically capture the micro-damage process in rocks. On the other hand, if the goal is to investigate the scale effects on peak strength at low confinements, then a homogenous, elastic BBM might be sufficient [89]. In any case, to use BBMs for predicting behavioral changes in rocks outside the set of conditions for which it is calibrated requires confidence that the model is a reasonable approximation of reality under the new set of conditions as well based on mechanistic logic. Accordingly, exercising prudence in interpreting and analyzing results and incorporating as much data as possible into the calibration process is paramount before using BBMs for predictive purposes.

7. Conclusions

Over the years, a number of different simplification (or model types) have been used in BBM studies for simulating the progressive damage process in granitic rocks, but the relative advantages and disadvantages of these model types are not well understood. To shed some light on this topic, this study has presented results for models of increasing complexity, and attempts were made to explain any data-model misfit on mechanistic grounds. Note that although the parameter space was explored extensively, we cannot definitively rule out the possibility that some other combination of parameters might produce similar macroscopic behavior, or that some parameter sets exist that could reproduce macroscopic behaviors more effectively than those identified in the paper. In any case, since these micromechanical models are physics-based, in that they try to capture the actual physics of rock damage, it was possible to identify physical reasons whenever some aspect of rock behavior could not be replicated.

It was found that block and contact heterogeneity must be incorporated in BBMs to allow for a realistic representation of the micro-fracturing process to be achieved. It was also established that the relative contribution of elastic block heterogeneity to the generation of tensile damage in the models is far more significant than that of contact heterogeneity. In terms of the representation of peak strength under high confinement conditions, it is important to assign an inelastic constitutive model to the block zones; this allows the zones to yield and soften and mimics the intragranular fracturing process. A heterogeneous block and contact BBM with inelastic zones could replicate not only the UCS and triaxial strengths but also the confined CIs, CDs, and the phenomenon of confinement-dependent dilatancy. Because this type of complex model has a large number of input parameters, it is important to utilize many target attributes from laboratory testing in the calibration process.

Lastly, the authors would like to acknowledge that a plane-strain model has been used here to study the behavior of three-dimensional rock specimens. The lack of an extra degree of freedom undoubtedly has some effect on the model results, but a corresponding three-dimensional study of this scope with realistic block size is currently not possible due to computational constraints. With further advances in computational capabilities and parallelization of 3DEC, it might be possible in future to replicate this study using 3D-BBMs.

Funding

The research conducted for this study was funded by the National Institute for Occupational Safety and Health (NIOSH) under Grant Number 200-2016-90154.

Declaration of Competing Interest

The authors declare that they have no known competing financial interests or personal relationships that could have appeared to influence the work reported in this paper.

Acknowledgement

The authors would like to extend their gratitude for the financial support. Special thanks to Dr. Mark Larson and Dr. Bo-Hyun Kim for reviewing this manuscript prior to submission and providing valuable suggestions.

Appendix A

See Fig. A1.

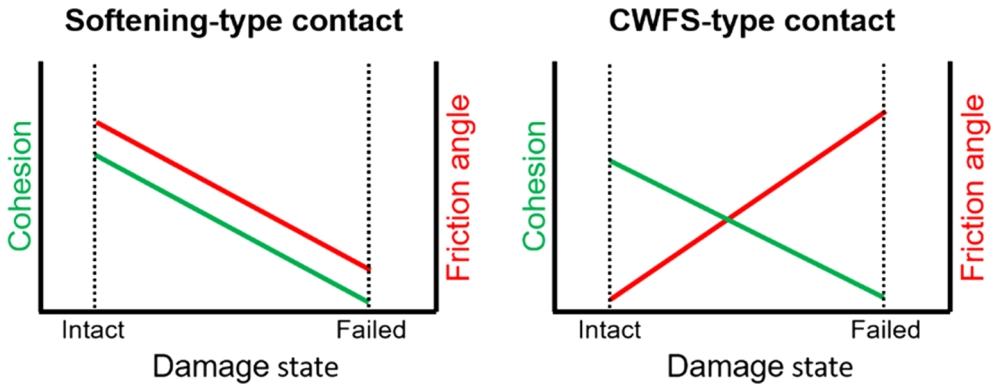

Fig. A1. Graphical description of the softening-type and CWFS-type contact behavior.

References

[1] Abdelaziz A, Zhao Q, Grasselli G. Grain based modelling of rocks using the combined finite-discrete element method. Comput Geotech 2018;103:73–81.

[2] Alejano LR, Alonso E. Considerations of the dilatancy angle in rocks and rock masses. Int J Rock Mech Min Sci 2005;42(4):481–507.

[3] Alejano LR, Posada D, Rodriguez-Dono A. Servo-controlled strength tests on moderately weathered granite. In: Proceedings of EUROCK Symposium, Rock eng. in difficult ground cond; 2009. P. 181–186.

[4] Arzúa J, Alejano LR. Dilation in granite during servo-controlled triaxial strength tests. Int J Rock Mech Min Sci 2013;61:43–56.
[5] Arzúa J, Alejano LR, Walton G. Strength and dilation of jointed granite specimens in servo-controlled triaxial tests. Int J Rock Mech Min Sci 2014;69:93–104.
[6] Bahaaddini M, Rahimi M. Distinct element modelling of the mechanical behaviour of intact rocks using Voronoi tessellation model. Int J Min Geo-Eng 2018;52(1):61–8.
[7] Bahrani N, Kaiser PK, Valley B. Distinct element method simulation of an analogue for a highly interlocked, non-persistently jointed rockmass. Int J Rock Mech Min Sci 2014;71:117–30.
[8] Bai Q, Tu S, Zhang C, Zhu D. Discrete element modeling of progressive failure of wide coal roadway from water-rich roofs. Int J Coal Geol 2016;167:215–29.
[9] Bass JD. Elasticity of minerals, glasses, and melts. Miner Phys Crystallogr: A Handbook Phys Const 1995;2:45–63.
[10] Bewick RP, Kaiser PK, Bawden WF. DEM simulation of direct shear: 2. Grain boundary and mineral grain strength component influence on shear rupture. Rock Mech Rock Eng 2014;47(5):1673–92.
[11] Bieniawski ZT. Mechanism of brittle fracture of rock: part I—theory of the fracture process. Int J Rock Mech Min Sci Geomech Abstr 1967;4(4):395–406.
[12] Bieniawski ZT, Bernede MJ. Suggested methods for determining the uniaxial compressive strength and deformability of rock materials: Part 1. Suggested method for determining deformability of rock materials in uniaxial compression. Int J Rock Mech Min Sci Geomech Abstr 1979;16(2):138–40.
[13] Blair SC, Cook NG. Analysis of compressive fracture in rock using statistical techniques: Part I. A non-linear rule-based model. Int J Rock Mech Min Sci 1998;35(7):837–48.
[14] Chang SH, Lee CI. Estimation of cracking and damage mechanisms in rock under triaxial compression by moment tensor analysis of acoustic emission. Int J Rock Mech Min Sci 2004;41(7):1069–86.
[15] Chen W, Konietzky H. Simulation of heterogeneity, creep, damage and lifetime for loaded brittle rocks. Tectonophysics 2014;633:164–75.
[16] Chen L, Liu JF, Wang CP, Liu J, Su R, Wang J. Characterization of damage evolution in granite under compressive stress condition and its effect on permeability. Int J Rock Mech Min Sci 2014;71:340–9.
[17] Chen W, Konietzky H, Tan X, Frühwirt T. Pre-failure damage analysis for brittle rocks under triaxial compression. Comput Geotech 2016;74:45–55.
[18] Cho NA, Martin CD, Sego DC. A clumped particle model for rock. Int J Rock Mech Min Sci 2007;44(7):997–1010.
[19] Christianson M, Board M, Rigby D. UDEC simulation of triaxial testing of lithophysal tuff. In: Proceedings of 41st US Symposium on Rock Mechanics; 2006.
[20] Coggan J, Gao F, Stead D, Elmo D. Numerical modelling of the effects of weak immediate roof lithology on coal mine roadway stability. Int J Coal Geol 2012;90:100–9.
[21] Cundall PA. A computer model for simulating progressive large-scale movements in blocky rock systems. In: Proceedings of Int. Society for Rock Mechanics Symposium: Rock Fracture; 1971. p. 129–136.
[22] Cundall PA, Strack ODL. A discrete numerical model for granular assemblies. Geotechnique 1979;29(1):47–65.
[23] Dey TN, Wang CY. Some mechanisms of microcrack growth and interaction in compressive rock failure. Int J Rock Mech Min Sci 1981;18:199–209.
[24] Diederichs MS. Instability of hard rock masses: the role of tensile damage and relaxation. Ph. D. Thesis. University of Waterloo, Waterloo; 1999.
[25] Diederichs MS. Rock fracture and collapse under low confinement conditions. Rock Mech Rock Eng 2003;36(5):339–81.
[26] Diederichs MS. The 2003 Canadian Geotechnical Colloquium: Mechanistic interpretation and practical application of damage and spalling prediction criteria for deep tunnelling. Can Geotech J 2007;44(9):1082–116.
[27] Diederichs MS and Martin CD. Measurement of spalling parameters from laboratory testing. In: Zhao Labiouse, DudtMathiereds. Rock Mechanics in Civil and Environmental Engineering. London: Taylor & Francis; 2010.
[28] Ding X, Zhang L. A new contact model to improve the simulated ratio of unconfined compressive strength to tensile strength in bonded particle models. Int J Rock Mech Min Sci 2014;69:111–9.
[29] Eberhardt E, Stead D, Stimpson B, Read RS. Identifying crack initiation and propagation thresholds in brittle rock. Can Geotech J 1998;35(2):222–33.
[30] Eberhardt E, Stead D, Stimpson B. Quantifying progressive pre-peak brittle fracture damage in rock during uniaxial compression. Int J Rock Mech Min Sci 1999;36(3):361–80.
[31] Eberhardt E, Stimpson B, Stead D. Effects of grain size on the initiation and propagation thresholds of stress-induced brittle fractures. Rock Mech Rock Eng 1999;32(2):81–99.
[32] Eberhardt E, Stimpson B, Stead D. The influence of mineralogy on the initiation of microfractures in granite. Proceedings of 9th ISRM Congress. 1999.
[33] Fabjan T, Mas Ivars D, Vukadin V. Numerical simulation of intact rock behaviour via the continuum and Voronoi tesselletion models: a sensitivity analysis. Acta Geotechnica Slovenica 2015;12(2):5–23.
[34] Fairhurst CE, Hudson JA. Draft ISRM suggested method for the complete stress-strain curve for intact rock in uniaxial compression. Int J Rock Mech Min Sci 1999;36(3):279–89.
[35] Farahmand K, Diederichs MS. A calibrated Synthetic Rock Mass (SRM) model for simulating crack growth in granitic rock considering grain scale heterogeneity of polycrystalline rock. In: Proceedings of 49th US Rock Mechanics/Geomechanics Symposium; 2015.
[36] Farahmand K, Vazaios I, Diederichs MS, Vlachopoulos N. Investigating the scale-dependency of the geometrical and mechanical properties of a moderately jointed rock using a synthetic rock mass (SRM) approach. Comput Geotech 2018;95:162–79.
[37] Fritzen F. Microstructural modeling and computational homogenization of the physically linear and nonlinear constitutive behavior of micro-heterogeneous materials. Karlsruhe: Kit Scientific Publishing; 2011.
[38] Gao FQ, Stead DO. The application of a modified Voronoi logic to brittle fracture modelling at the laboratory and field scale. Int J Rock Mech Min Sci 2014;68:1–14.
[39] Gao F, Stead D, Elmo D. Numerical simulation of microstructure of brittle rock using a grain-breakable distinct element grain-based model. Comput Geotech 2016;78:203–17.
[40] Gao M, Liang Z, Li Y, Wu X, Zhang M. End and shape effects of brittle rock under uniaxial compression. Arabian J Geosci 2018;11(20):614.
[41] Gallagher JJ, Friedman M, Handin J, Sowers GM. Experimental studies relating to microfractures in sandstone. Tectonophysics 1974;21:203–47.
[42] Garza-Cruz TV, Pierce M and Kaiser PK. Use of 3DEC to study spalling and deformation associated with tunnelling at depth. In: Proceedings of the Seventh International Conference on Deep and High Stress Mining; 2014. p. 421–34.
[43] Garza-Cruz, Pierce ME. A 3DEC model for heavily veined massive rock masses. In: Proceedings of 48th US Rock Mechanics/Geomechanics Symposium; 2014.
[44] Ghazvinian E. Modeling and testing strategies for brittle fracture simulation in crystalline rock samples. M.A.Sc Thesis. Queen's University, Ontario, Canada; 2010.
[45] Ghazvinian E, Diederichs MS, Quey R. 3D random Voronoi grain-based models for simulation of brittle rock damage and fabric-guided micro-fracturing. J Rock Mech Geotech Eng 2014;6(6):506–21.
[46] Haimson B, Chang C. A new true triaxial cell for testing mechanical properties of rock, and its use to determine rock strength and deformability of Westerly granite. Int J Rock Mech Min Sci 2000;37(1–2):285–96.
[47] Hemami B, Fakhimi A. Numerical simulation of rock-loading machine interaction. In: Proceedings of 48th US Rock Mechanics/Geomechanics Symposium; 2014.
[48] Hoek E, Brown ET. Empirical strength criterion for rock masses. J Geotech Geoenviron Eng 1980;106.
[49] Hofmann H, Babadagli T, Yoon JS, Zang A, Zimmermann G. A grain based modeling study of mineralogical factors affecting strength, elastic behavior and micro fracture development during compression tests in granites. Eng Fract Mech 2015;147:261–75.
[50] Hugman RHH, Friedman M. Effects of texture and composition on mechanical behavior of experimentally deformed carbonate rocks. Am Assoc Pet Geol Bull 1979;63:1478–89.
[51] Itasca. UDEC Version 6.0: Theory and Background. Itasca Consulting Group Inc. Minneapolis, Minnesota; 2014.
[52] Kazerani T, Zhao J. Micromechanical parameters in bonded particle method for modelling of brittle material failure. Int J Numer Anal Meth Geomech 2010;34(18):1877–95.
[53] Kranz RL. Microcracks in rocks: a review. Tectonophysics 1983;100(1–3):449–80.
[54] Lan H, Martin CD, Hu B. Effect of heterogeneity of brittle rock on micromechanical extensile behavior during compression loading. J Geophys Res: Solid Earth 2010;115(B1).
[55] Li H, Li K, Subhash G, Kecskes LJ, Dowding RJ. Micromechanical modeling of tungsten-based bulk metallic glass matrix composites. Mat Sci Eng 2006;A429:115–23.
[56] Li J, Konietzky H, Frühwirt T. Voronoi-based DEM simulation approach for sandstone considering grain structure and pore size. Rock Mech Rock Eng 2017;50(10):2749–61.
[57] Li XF, Li HB, Zhao J. The role of transgranular capability in grain-based modelling of crystalline rocks. Comput Geotech 2019;110:161–83.
[58] Lisjak A, Tatone BS, Mahabadi OK, Grasselli G, Marschall P, Lanyon GW, et al. Hybrid finite-discrete element simulation of the EDZ formation and mechanical sealing process around a microtunnel in Opalinus Clay. Rock Mech Rock Eng 2016;49(5):1849–73.
[59] Liu G, Cai M, Huang M. Mechanical properties of brittle rock governed by micro-geometric heterogeneity. Comput Geotech 2018;104:358–72.
[60] Lee SE, Kim MI, Park JH, Park CK, Kang M, Jeong GC. Damage process of intact granite under uniaxial compression: microscopic observations and contact stress analysis of grains. Geosci J 2006;10(4):457–63.
[61] Mahabadi OK. Investigating the influence of micro-scale heterogeneity and microstructure on the failure and mechanical behaviour of geomaterials. Doctoral dissertation; 2012.
[62] Mahabadi O, Randall N, Zong Z, Grasselli G. A novel approach for micro-scale characterization and modeling of geomaterials incorporating actual material heterogeneity. Geophys Res Lett 2012;39(1).
[63] Mahabadi OK, Tatone BS, Grasselli G. Influence of microscale heterogeneity and microstructure on the tensile behavior of crystalline rocks. J Geophys Res Solid Earth 2014;119(7):5324–41.
[64] Martin CD, Chandler NA. The progressive fracture of Lac du Bonnet granite. Int J Rock Mech Min Sci Geomech Abstr 1994;31(6):643–59.
[65] Mas Ivars D, Potyondy DO, Pierce M, Cundall PA. The smooth-joint contact model. In: Proceedings of WCCM8-ECCOMAS; 2008.
[66] Mavko G, Mukerji T, Dvorkin J. The rock physics handbook: Tools for seismic analysis of porous media. Cambridge University Press; 2009.
[67] Mayer JM, Stead D. Exploration into the causes of uncertainty in UDEC grain boundary models. Comput Geotech 2017;82:110–23.
[68] Mogi K. Experimental Rock Mechanics. CRC Press; 2006.
[69] Moore DE, Lockner DA. The role of microcracking in shear-fracture propagation in granite. J Struct Geol 1995;17(1):95–114.
[70] Munjiza AA. The Combined Finite-Discrete Element Method. John Wiley & Sons; 2004.

[71] Nicksiar M, Martin CD. Factors affecting crack initiation in low porosity crystalline rocks. Rock Mech Rock Eng 2014;47(4):1165–81.
[72] Noorani R, Cai M. Simulation of dilation behavior of brittle rocks using a grain-based model. In: Proceedings of 13th ISRM International Congress of Rock Mechanics; 2015.
[73] Norouzi S, Baghbanan A, Khani A. Investigation of grain size effects on micro/macro-mechanical properties of intact rock using Voronoi element—discrete element method approach. Part Sci Technol 2013;31(5):507–14.
[74] Olsson WA. Grain size dependence of yield stress in marble. J Geophys Res 1974;79(32):4859–62.
[75] Park JW, Park C, Song JW, Park ES, Song JJ. Polygonal grain-based distinct element modeling for mechanical behavior of brittle rock. Int J Numer Anal Meth Geomech 2017;41(6):880–98.
[76] Peng J, Wong LN, Teh CI, Li Z. Modeling micro-cracking behavior of Bukit Timah granite using grain-based model. Rock Mech Rock Eng 2018;51(1):135–54.
[77] Peng J, Rong G, Jiang M. Variability of crack initiation and crack damage for various rock types. Arabian J Geosci 2018;11(11):265.
[78] Perras MA, Diederichs MS. A review of the tensile strength of rock: concepts and testing. Geotech Geol Eng 2014;32(2):525–46.
[79] Potyondy DO, Cundall PA, Lee CA. Modelling rock using bonded assemblies of circular particles. In: Proceedings of 2nd North American Rock Mechanics Symposium; 1996.
[80] Potyondy DO. A flat-jointed bonded-particle material for hard rock. In: Proceedings of 46th US Rock Mechanics/Geomechanics Symposium; 2012.
[81] Potyondy DO, Cundall PA. A bonded-particle model for rock. Int J Rock Mech Min Sci 2004;41(8):1329–64.
[82] Preston RP, Stead D, McIntire H and Roberts DP. Quantifying the effects of adverse geology on pillar strength through numerical modeling. In: Proceedings of 47th US Rock Mechanics/Geomechanics Symposium; 2013.
[83] Scholtès L, Donzé FV. A DEM model for soft and hard rocks: role of grain interlocking on strength. J Mech Phys Solids 2013;61(2):352–69.
[84] Shen B. Coal mine roadway stability in soft rocks: a case study. Rock Mech Rock Eng 2014;47:2225–38.
[85] Sinha S and Walton G. Application of micromechanical modeling to prediction of in-situ rock behavior. In: Proceedings of 52nd US Rock Mechanics/Geomechanics Symposium; 2018.
[86] Sinha S, Walton G. Understanding continuum and discontinuum models of rock-support interaction for excavations undergoing stress-induced spalling. Int J Rock Mech Min Sci 2019;R1. submitted for publication.
[87] Sinha S, Walton G. Simulating laboratory-scale damage in granite using Bonded Block Models (BBM). In: Proceedings of 14th International Congress on Rock Mechanics and Rock Engineering; 13–18 September, 2019b.
[88] Sprunt ES, Brace WF. Direct observation of microcavities in crystalline rocks. Int J Rock Mech Min Sci Geomech Abstr 1974;11(4):139–50.
[89] Stavrou A, Murphy W. Quantifying the effects of scale and heterogeneity on the confined strength of micro-defected rocks. Int J Rock Mech Min Sci 2018;102:131–43.
[90] Tapponnier P, Brace WF. Development of stress-induced microcracks in Westerly granite. Int J Rock Mech Min Sci Geomech Abstr 1976;13(4):103–12.
[91] Tan X, Konietzky H, Chen W. Numerical simulation of heterogeneous rock using discrete element model based on digital image processing. Rock Mech Rock Eng 2016;49(12):4957–64.
[92] Vermeer PA, De Borst R. Non-associated plasticity for soils, concrete and rock. HERON. 1984;29 (3).
[93] Walton G. Improving continuum models for excavations in rock masses under high stress through an enhanced understanding of post-yield dilatancy. Ph.D. Thesis. Queen's University, Kingston, Canada; 2014.
[94] Walton G, Diederichs MS. A new model for the dilation of brittle rocks based on laboratory compression test data with separate treatment of dilatancy mobilization and decay. Geotech Geol Eng 2015;33(3):661–79.
[95] Walton G, Arzua J, Alejano LR, Diederichs MS. A laboratory-testing-based study on the strength, deformability, and dilatancy of carbonate rocks at low confinement. Rock Mech Rock Eng 2015;48(3):941–58.
[96] Walton G, Diederichs M, Punkkinen A, Whitmore J. Back analysis of a pillar monitoring experiment at 2.4 km depth in the Sudbury Basin Canada. Int J Rock Mech Min Sci 2016;85:33–51.
[97] Walton G, Hedayat A, Kim E, Labrie D. Post-yield strength and dilatancy evolution across the brittle–ductile transition in Indiana limestone. Rock Mech Rock Eng 2017;50(7):1691–710.
[98] Wang X, Cai M. Modeling of brittle rock failure considering inter-and intra-grain contact failures. Comput Geotech 2018;101:224–44.
[99] Wang X, Cai M. A comprehensive parametric study of grain-based models for rock failure process simulation. Int J Rock Mech Min Sci 2019;115:60–76.
[100] Wong TF. Micromechanics of faulting in Westerly Granite. Int J Rock Mech Min Sci 1982;19:49–64.
[101] Wong RH, Chau KT, Wang P. Microcracking and grain size effect in Yuen Long marbles. Int J Rock Mech Min Sci Geomech Abstr 1996;33(5):479–85.
[102] Wong TF, Wong RHC, Chau KT, Tang CA. Microcrack statistics, Weibull distribution and micromechancial modeling of compressive failure in rock. Mech Mater 2006;38:664–81.
[103] Xue L, Qin S, Sun Q, Wang Y, Lee LM, Li W. A study on crack damage stress thresholds of different rock types based on uniaxial compression tests. Rock Mech Rock Eng 2014;47(4):1183–95.
[104] Yuan SC, Harrison JP. An empirical dilatancy index for the dilatant deformation of rock. Int J Rock Mech Min Sci 2004;4(41):679–86.
[105] Zhou J, Lan H, Zhang L, Yang D, Song J, Wang S. Novel grain-based model for simulation of brittle failure of Alxa porphyritic granite. Eng Geol 2019;251:100–14.
[106] Zhao XG, Cai M. A mobilized dilation angle model for rocks. Int J Rock Mech Min Sci 2010;47(3):368–84.
[107] Zhao XG, Cai M, Wang J, Ma LK. Damage stress and acoustic emission characteristics of the Beishan granite. Int J Rock Mech Min Sci 2013;64:258–69.